Cancer & Metabolism

RESEARCH Open Access

Identification and impact of microbiota-derived metabolites in ascites of ovarian and gastrointestinal cancer

Sisi Deng[1,2,3,4], Wooyong Kim[3,4], Kefan Cheng[3,4], Qianlu Yang[1], Yogesh Singh[5], Gyuntae Bae[1,2], Nicolas Bézière[1,7], Lukas Mager[2,4,7,8,9], Stefan Kommoss[6], Jannik Sprengel[3,4] and Christoph Trautwein[1,2,3,4*]

Abstract

Background Malignant ascites is a common complication of advanced ovarian cancer (OC) and gastrointestinal cancer (GI), significantly impacting metastasis, quality of life, and survival. Increased intestinal permeability can lead to blood or lymphatic infiltration and microbial translocation from the gastrointestinal or uterine tract. This study aimed to identify microbiota-derived metabolites in ascites from OC (stages II-III and IV) and GI patients, assessing their roles in tumor progression.

Methods Malignant ascites samples from 18 OC and GI patients were analyzed using a four-dimensional (4D) untargeted metabolomics approach combining reversed-phase (RP) and hydrophilic interaction liquid chromatography (HILIC) with trapped ion mobility spectrometry time-of-flight mass spectrometry (timsTOF-MS). Additonally, a targeted flow cytometry-based cytokine panel was used to screen for inflammatory markers. Non-endogenous, microbiota-derived metabolites were identified through the Human Microbial Metabolome Database (MiMeDB).

Results OC stage IV exhibited metabolic profiles similar to GI cancers, while OC stage II-III differed significantly. Stage IV OC patients exhibited higher levels of 11 typically microbiome-derived metabolites, including 1-methylhistidine, 3-hydroxyanthranilic acid, 4-pyridoxic acid, biliverdin, butyryl-L-carnitine, hydroxypropionic acid, indole, lysophosphatidylinositol 18:1 (LPI 18:1), mevalonic acid, N-acetyl-L-phenylalanine, and nudifloramide, and lower levels of 5 metabolites, including benzyl alcohol, naringenin, o-cresol, octadecanedioic acid, and phenol, compared to stage II–III. Correlation analysis revealed positive associations between IL-10 and metabolites such as glucosamine and LPCs, while MCP-1 positively correlated with benzyl alcohol and phenol.

Conclusion 4D metabolomics revealed distinct metabolic signatures in OC and GI ascites, highlighting microbiota-derived metabolites involved in lipid metabolism and inflammation. Metabolites like 3-hydroxyanthranilic acid, indole, and naringenin may serve as markers of disease progression and underscore the microbiota's role in shaping malignant ascites and tumor biology.

Keywords Microbiota, Malignant Ascites, TimsTOF, Flow cytometry, MiMeDB

*Correspondence:
Christoph Trautwein
christoph.trautwein@med.uni-tuebingen.de

Full list of author information is available at the end of the article

© The Author(s) 2025. **Open Access** This article is licensed under a Creative Commons Attribution-NonCommercial-NoDerivatives 4.0 International License, which permits any non-commercial use, sharing, distribution and reproduction in any medium or format, as long as you give appropriate credit to the original author(s) and the source, provide a link to the Creative Commons licence, and indicate if you modified the licensed material. You do not have permission under this licence to share adapted material derived from this article or parts of it. The images or other third party material in this article are included in the article's Creative Commons licence, unless indicated otherwise in a credit line to the material. If material is not included in the article's Creative Commons licence and your intended use is not permitted by statutory regulation or exceeds the permitted use, you will need to obtain permission directly from the copyright holder. To view a copy of this licence, visit http://creativecommons.org/licenses/by-nc-nd/4.0/.

Statement of translational relevance.

Ascites is a hallmark of advanced gynecological and gastrointestinal cancers with peritoneal metastasis, often associated with poor overall survival. Intraperitoneal chemotherapy (IPC), including hyperthermic intraperitoneal chemotherapy (HIPEC) and pressurized intraperitoneal aerosol chemotherapy (PIPAC), is widely used in clinical practice, showing promising outcomes such as 63.3% pain relief and 60% ascites resolution. However, enhancing IPC efficacy while minimizing toxicity remains a critical challenge. Emerging evidence highlights the role of gut microbiota modulation—through fecal microbiota transplantation (FMT), prebiotics, probiotics, antibiotics, and dietary interventions—in improving chemotherapy and Immune Checkpoint Inhibitors (ICI) sensitivity and overcoming drug resistance. Profiling microbiota-derived metabolites in malignant ascites across cancer stages and types could reveal tumor regression-associated changes and provide insights into targeted combination therapies. Integrating FMT, ICI with IPC has the potential to amplify therapeutic effects, offering a novel translational approach to optimize treatment outcomes for patients with advanced cancers and ascites.

Introduction

Ovarian cancer (OC) is a leading cause of cancer-related mortality among women and is often termed the "silent killer" due to its asymptomatic nature in the early stages and lack of effective screening tools [1, 2]. Consequently, most OC cases are diagnosed at advanced stages when the disease has metastasized, limiting treatment options and resulting in a poor prognosis [3]. A common feature of advanced OC is the abnormal accumulation of fluid in the abdominal cavity, known as ascites, which significantly contributes to patient mortality [4]. Ascites not only serves as a clinical hallmark of OC but is also observed in other malignancies such as gastrointestinal (GI) cancers and cirrhosis, and is rarely associated with non-cancerous conditions like heart failure and peritoneal tuberculosis [5, 6].

The pathogenesis of ascites is multifactorial, involving hypoalbuminemia, increased vascular permeability, impaired lymphatic drainage, and fluid retention due to activation of the renin–angiotensin–aldosterone system (RAAS) [7–9]. Recent research has highlighted the role of the gut microbiota in modulating these processes through its influence on immune and metabolic pathways. For instance, butyrate produced by gut bacteria can inhibit RAAS activity, reducing fluid retention [10–12]. Disruption of gut microbial balance in advanced disease may exacerbate intestinal permeability and promote bacterial translocation [13–17], contributing to ascites formation and creating a vicious cycle of inflammation and fluid accumulation.

One of the main complications of ascites is bacterial peritonitis (BP), which has been well-documented in patients with GI malignancies [18, 19]. BP is often spontaneous and linked to bacterial translocation from the GI tract to the mesenteric lymph nodes [20]. While less frequently reported in OC, the extensive metastasis and abdominal involvement in advanced OC may similarly compromise gastrointestinal integrity, increasing susceptibility to BP. The partially overlapping features of ascites in OC and GI cancers raise questions about the potential role of the microbiome in shaping the tumor-promoting properties of this fluid.

Moreover, ascites is not just a passive by-product of malignancy but may actively shape the tumor microenvironment, promoting metastasis and therapeutic resistance [21, 22]. Its heterogeneous nature — ranging from clear and free-flowing to viscous and loculated — indicates distinct underlying biological processes that could influence tumor behavior. While paracentesis provides temporary symptomatic relief, it is often palliative and requires repeated procedures, carrying risks such as infection and protein loss. Despite its clinical significance, the molecular and microbial landscape of OC-associated ascites remains poorly understood.

Reversed-phase (RP) and hydrophilic interaction liquid chromatography (HILIC) coupled with trapped ion mobility time-of-flight mass spectrometry (timsTOF) were employed for a fully untargeted four-dimensional (4D) metabolomics analysis of ascitic fluid. Flow cytometry was used to profile inflammatory cytokines. Microbiota-derived metabolites were identified through the Human Microbial Metabolome Database (MiMeDB). These approaches aimed to characterize the metabolic and cytokine profiles of ascitic fluid and evaluate the potential impact of microbiota-derived metabolites on OC and GI progression.

Materials and methods

This exploratory study included 10 malignant ascites specimens from patients undergoing ovarian cancer (OC) resection and 8 malignant ascites specimens from gastrointestinal (GI) cancers patients. Metabolomics and cytokine analysis were used to combine the results for in-depth phenotyping of malignant ascites.

Ethical background

This study was conducted in accordance with the principles outlined in the Declaration of Helsinki and approved by the Ethics Committee, Faculty of Medicine, University of Tübingen, Germany (Ref. Nr. 696/2016BO2 and 117/2020BO1). Written informed consent was obtained from all participating patients. The collection of samples did not interfere with or alter patient treatment plans. All data were anonymized in compliance with the European

General Data Protection Regulation (GDPR) and applicable German data protection laws.

Collection and storage of ascitic fluid samples

Ascites samples were collected from patients undergoing surgery for ovarian cancer at the Department of General and Transplant Surgery and the Women's Hospital, University Hospital Tübingen, Germany. Samples were obtained under sterile conditions in the operating room, stored in sterile tubes, and immediately transported to the laboratory using an icebox to maintain low temperatures. Upon arrival, the samples were centrifuged at 4 °C for 30 minutes at 1,200 rpm. The resulting supernatant was aliquoted into 2 mL tubes and stored at – 80 °C until further analysis. Relevant patient information, including demographic data, cancer histology, and the extent of peritoneal disease was recorded. All samples and associated patient data were anonymized prior to analysis.

Quantification of cytokines in malignant Ascites

To quantify cytokine levels in malignant ascites, 25 µL of ascites from ovarian cancer patients was mixed with 25 µL of assay buffer. Next, 25 µL of a 13-plex bead mix from the LEGENDplex™ Human Inflammation Panel 1 (13-plex, #740809, BioLegend, USA) was added to each well of a 96-well microplate. This multiplex bead-based assay is capable of quantifying 13 different cytokines/chemokines with the following minimum detectable concentrations (MDC) in parentheses: IL-1β (1.5 ± 0.6 pg/mL), IFN-α2 (2.1 ± 0.2 pg/mL), IFN-γ (1.3 ± 1.0 pg/mL), TNF-α (0.9 ± 0.8 pg/mL), MCP-1 (1.1 ± 1.2 pg/mL), IL-6 (1.5 ± 0.7 pg/mL), IL-8 (2.0 ± 0.5 pg/mL), IL-10 (2.0 ± 0.5 pg/mL), IL-12p70 (2.0 ± 0.2 pg/mL), IL-17 A (0.5 ± 0.0 pg/mL), IL-18 (2.0 ± 0.5 pg/mL), IL-23 (1.8 ± 0.1 pg/mL), and IL-33 (4.4 ± 1.5 pg/mL).

The plate was incubated and shaken at room temperature for 2 h, allowing the analytes (cytokines) to bind to the corresponding antibody-conjugated capture beads. Following incubation, the wells were washed to remove unbound analytes. Biotinylated detection antibodies (25 µL) were then added and allowed to bind to the analyte-bound beads. After 30 min of incubation, 25 µL of streptavidin–phycoerythrin (SA-PE) was added, which binds to the biotinylated detection antibodies and produces a fluorescent signal proportional to the amount of each cytokine.

After a further 1-hour incubation, the beads were washed, resuspended in wash buffer, and samples were acquired using a flow cytometer. Fluorescent signals were measured, and the concentrations of the analytes were determined based on standard curves generated using the LEGENDplex™ data analysis software (BioLegend, USA).

Sample Preparation for timsTOF LC-MS analysis

Frozen ascites samples were thawed at room temperature, and 1.2 mL of each sample was transferred into separate 1.5 mL Eppendorf tubes. The tubes were centrifuged at 14,000 rpm at 4 °C for 15 minutes. The supernatants (1 mL) were carefully collected and evaporated at room temperature using a Concentrator Plus (Eppendorf, Wesseling-Berzdorf, Germany) for 6 hours.

Reversed-Phase Liquid Chromatography (RPLC) sample Preparation

For reversed-phase (RP) liquid chromatography analysis, the dried samples were reconstituted in 100 µL of MilliQ water (MQ) and 300 µL of ice-cold (-20 °C) high-performance liquid chromatography (HPLC) grade acetonitrile (VWR Chemicals, Darmstadt, Germany). The mixture was vortexed for 1 minute, followed by incubation at -20 °C for 10 minutes. Samples were then centrifuged at 14,000 rpm at 4 °C for 15 min. From each tube, 300 µL of the supernatant was transferred to a new Eppendorf tube and evaporated to dryness for 1.5 hours at room temperature. The dried samples were then reconstituted in 60 µL of MQ/acetonitrile (9:1, v/v), vortexed for 10 s, and centrifuged again at 14,000 rpm at 4 °C for 15 min. Finally, 50 µL of the supernatant was transferred to HPLC vials (VWR, Leuven, Belgium) equipped with inserts for subsequent RPLC-MS analysis.

Hydrophilic Interaction Liquid Chromatography (HILIC) sample Preparation

For hydrophilic interaction liquid chromatography (HILIC) analysis, the dried samples were reconstituted in 100 µL of MQ and 300 µL of ice-cold (-20 °C) acetonitrile. The mixture was vortexed for 1 minute, followed by incubation at -20 °C for 10 minutes. The samples were centrifuged at 14,000 rpm at 4 °C for 15 minutes, and the resulting supernatant (300 µL) was transferred into HPLC vials with inserts for HILIC-MS measurements.

Liquid chromatography conditions

Analyte separation was performed using the Elute PLUS LC series (Bruker, Bremen, Germany).

RPLC conditions

RPLC separations were conducted on an Intensity Solo 2 C18 Column (100 Å; 2.0 µm; 2.1 mm × 100 mm; #BRHSC18022100, Bruker) using 0.1% formic acid in MilliQ water as mobile phase A and 0.1% formic acid in acetonitrile as mobile phase B. A 5 µL injection of each sample was used. The separation was carried out at a flow rate of 0.4 mL/min from 0 to 9 min and 10.6 to 13 min, and at 0.6 mL/min from 9.1 to 10.6 min, with a column temperature maintained at 50 °C using the following gradient: 0–1 min, 5% B; 1–7 min, 5–40% B; 7–9 min,

40–98% B; 9–10.6 min, 98% B; 10.6–10.7 min, 98 – 5% B; 10.7–13 min, 5% B.

HILIC conditions

HILIC separations were performed on an ACQUITY UPLC BEH Amide column (130 Å, 1.7 µm, 2.1 mm × 150 mm; #186004802, Waters) using 10 mM ammonium formate and 0.1% formic acid in MilliQ water as mobile phase A and 10 mM ammonium formate and 0.1% formic acid in acetonitrile as mobile phase B. A 5 µL injection was used, with separation conducted at a flow rate of 0.5 mL/min and a column temperature of 40 °C using the following gradient: 0–3 min, 100% B; 3–10 min, 100 –85% B; 10–14 min, 85 – 50% B; 14–15 min, 50% B; 15–15.1 min, 50–100% B; 15.1–23 min, 100% B.

Mass spectrometry analysis

The separated analytes were analyzed using a timsTOF fleX mass spectrometer (Bruker, Bremen, Germany) equipped with an Apollo II source for RP measurements, and a timsTOF Pro 2 (Bruker, Bremen, Germany) with a vacuum-insulated probe heated electrospray ionization (VIP-HESI) source for HILIC analysis. LC-MS/MS data were acquired in duplicate (technical replicates) using positive and negative dda-PASEF modes, with a TOF mass range of m/z 20-1300. Default Bruker PASEF acquisition parameters for MS/MS acquisition were used: 2 ramps (12 precursors each) per cycle; resulting cycle time 0.69 s; Intensity threshold 100 counts; Target Intensity 4000 counts (signals below that threshold will be scheduled for MS/MS fragmentation more often); Active Exclusion activated (0.1 min; reconsider if intensity increase is 2-fold or higher). The system was controlled using timsControl® and Compass HyStar® software, and data acquisition was managed using the same software. Quality control (QC) samples were run every ten injections, and blank samples were analyzed using H_2O for RP and acetonitrile for HILIC.

Data preprocessing and statistical analysis

Raw data processing was conducted using MetaboScape® software (version 2024b, Bruker, RRID: SCR_026044) with four-dimensional (4D) feature extraction, capturing mass-to-charge ratio (m/z), isotopic pattern quality, retention times, MS/MS spectra, and collision cross-section (CCS) values. Feature extraction was performed using the T-ReX® 4D algorithm (RRID: SCR_026044), followed by annotation through the Bruker Human Metabolome Database (HMDB, RRID: SCR_007712) and the NIST Mass Spectral Library (RRID: SCR_014668) Level 2 annotation according to *Sumner et al.* [23]. High-quality spectra were selected based on stringent criteria, including chromatogram and ion mobilogram quality, annotation scores, and CCS accuracy (Table S3). Potential microbiota-derived metabolites were identified and their origins traced to specific microbiota species using the Human Microbial Metabolome Database (MiMeDB, RRID: SCR_025108).

Data from RP and HILIC measurements were integrated for analysis. Sample intensities from omic data were normalized using probabilistic quotient normalization (PQN), log-transformed, and scaled using Pareto scaling to approximate normality. The final dataset was analyzed and visualized using MetaboAnalystR (RRID: SCR_016723), Pheatmap (RRID: SCR_016418), and ComplexHeatmap (RRID: SCR_017270) packages in R (version 4.3.2). Descriptive statistics and correlation analyses were performed in R. Comparative statistics included t-tests and one-way analysis of variance (ANOVA) for normally distributed data, and non-parametric tests for skewed data.

Results

Patients' clinical characteristics

Ascites samples were collected from 10 OC and 8 GI patients undergoing open surgery for malignancy removal. The clinicopathological characteristics of the patients are summarized in Table 1. None of the OC patients had received chemotherapeutic treatment before ascites collection. Notably, the OC patient with clear cell carcinoma did not have a history of endometriosis. Two of the GI patients had previously received neoadjuvant chemotherapy, and all had peritoneal metastases. Due to the limited sample size and the heterogeneity in histological subtypes and cancer origins, all available GI patient data were included to provide a general overview. Despite the treatment history in a subset of GI patients, the observed differences remain relevant and informative.

Metabolite differences between Ovarian Cancer (Stages II-III, IV) and Gastrointestinal Cancer groups

Distinct metabolite changes were observed between OC stages II-III and GI groups, while ovarian cancer stage IV samples displayed metabolic profiles equivalent to those of the GI cancer samples (Fig. 1A). Normalized intensity data from three groups—OC II-III (ovarian cancer stages II-III), OC IV (ovarian cancer stage IV), and GI (including appendiceal, colon, and gastric cancers)—were analyzed using one-way ANOVA with a false discovery rate (FDR, Benjamini-Hochberg) cutoff of 0.05 (Table S4.1 and S4.2). Twelve significant metabolites were identified out of the 696 measured. Approximately 92% of the metabolites showed distinct intensity distributions when comparing the GI group with the OC II-III group. However, when comparing the GI group with OC IV, around 83% of the metabolites exhibited similar intensity trends (Fig. 1A).

Table 1 Clinic-pathological characteristics of the explorative cohort

	Ovarian cancer (OC)		Gastrointestinal (GI) cancers	
Number of patients	10		8	
Age (years)	64.6 ± 10.25		51.5 ± 18.34	
Gender Ratio (Female/male)	10/0 (100%)		7/1 (87.5%)	
Histology	High-grade serous carcinoma [*n* (%)]	8 (80)	Appendiceal signet ring cell carcinoma	1 (12.5)
			Low-grade appendiceal mucinous neoplasm	3 (37.5)
	Low-grade serous carcinoma [*n* (%)]	1 (10)	Colon adenocarcinoma	1 (12.5)
	Clear cell carcinoma [*n* (%)]	1 (10)	Gastric adenocarcinoma	3 (37.5)
Federation of gynecology and obstetrics stage (FIGO)	Stage II [*n* (%)]	1 (10)	/	
	Stage III [*n* (%)]	6 (60)		
	Stage IV [*n* (%)]	3 (30)		
T Stage				
T2 [*n* (%)]	1 (10)		/	
T3 [*n* (%)]	7 (70)		3 (37.5)	
T4 [*n* (%)]	/		5 (62.5)	
Tx [*n* (%)]	2 (20)		/	
N Stage				
N0 [*n* (%)]	4 (40)		3 (37.5)	
N1 [*n* (%)]	5 (50)		1 (12.5)	
N2 [*n* (%)]	/		2 (25)	
N3 [*n* (%)]	/		1 (12.5)	
Nx [*n* (%)]	1 (10)		1 (12.5)	
M Stage				
M0 [*n* (%)]	4 (40)		1 (12.5)	
M1 [*n* (%)]	2 (20)		6 (75)	
Mx [*n* (%)]	4 (40)		1 (12.5)	

Data are expressed as (mean ± standard) deviation or *n* (%)

The top 12 significant metabolites identified in the heatmap were further visualized using individual raincloud plots (Fig. 1B). Ten metabolites exhibited similar trends, with propofol-β-D-glucuronide (j.) showing a stepwise and significant decrease across the OC II-III, OC IV, and GI groups (OC IV significantly decreased compared to OC II-III, and GI significantly decreased compared to both OC II-III and OC IV).

Several metabolites, including 2-tert-butyl-4-ethylphenol (a.), 3-methoxy-4-(2-methylpropoxy) benzoic acid (b.), 4-isopropyl-3-methylphenol (d.), 4-prop-1-enylveratrole (e.), cuminaldehyde (f.), PPA (i.), and thymol (l.), exhibited a similar trend: OC IV showed a significant decrease compared to OC II-III, while GI significantly decreased compared to OC II-III. Although the GI group also decreased compared to OC IV, the difference was not statistically significant. Additionally, 4-(2,5-dimethylphenyl)-4-oxobutanoic acid (c.) and Glu-Gly-Arg (g.) showed significant decreases only when comparing GI to OC II-III, with no significant differences observed between OC IV and OC II-III or GI and OC IV.

In contrast, phenylalanylphenylalanine (h.) and SM 36:3;O2 (k.) followed a different pattern. Phenylalanylphenylalanine (h.) significantly increased in OC IV compared to both OC II-III and GI. SM 36:3;O2 (k.) exhibited a similar trend, though the difference between OC II-III and OC IV was not statistically significant.

A Venn diagram was generated to visualize the shared and unique metabolites among the OC II–III, OC IV, and GI groups, providing an overview of group-specific and overlapping metabolic features (Figure S3). Specifically, 12 metabolites were shared between OC II–III and OC IV only, 87 between OC II–III and GI only, and 40 between OC IV and GI only, while 785 metabolites were common to all three groups. In terms of unique metabolites, 13 were specific to OC II–III, 46 to OC IV, and 76 to the GI group. Detailed information is provided in Supplementary Tables S9.1 and S9.2.

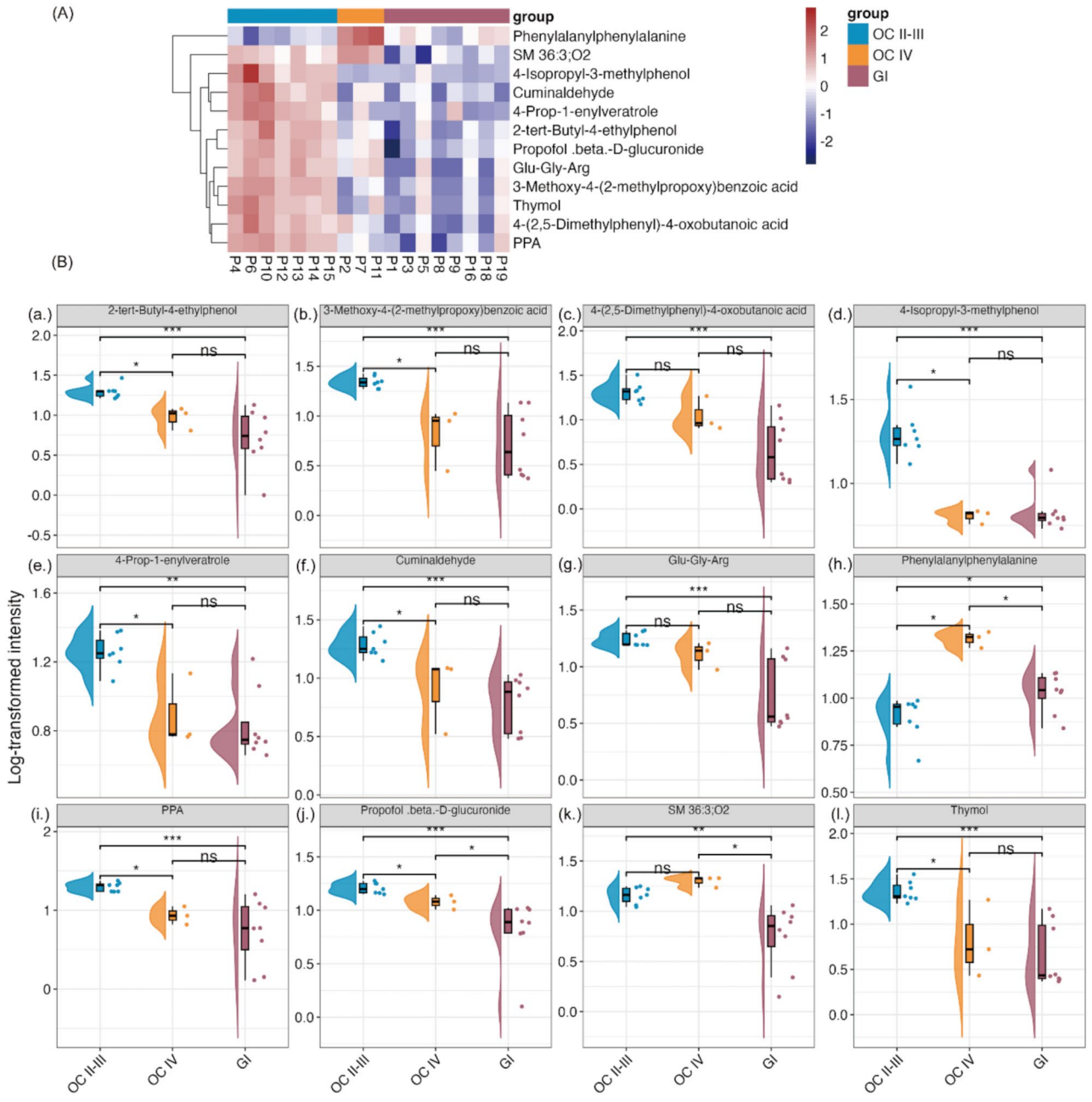

Fig. 1 Identification of Ascites Metabolic Signatures in OC II-III, OC IV, and GI Groups. (**A**) The heatmap displays significant metabolites identified through ANOVA (adjusted *p*-value cutoff of 0.05) across eight GI, seven OC II-III, and three OC IV biological replicates. Clustering was performed using Ward's hierarchical method with Euclidean distance as the distance metric. **(B)** Raincloud plots (combining violin, box, and strip plots) illustrate the significant metabolites: (**a**) 2-tert-butyl-4-ethylphenol, (**b**) 3-methoxy-4-(2-methylpropoxy)benzoic acid, (**c**) 4-(2,5-dimethylphenyl)-4-oxobutanoic acid, (**d**) 4-isopropyl-3-methylphenol, (**e**) 4-prop-1-enylveratrole, (**f**) cuminaldehyde, (**g**) Glu-Gly-Arg, (**h**) phenylalanylphenylalanine. (**i**) PPA, (**j**) Propofol-β-D-glucuronide, (**k**) SM 36:3;O2, and (**l**) thymol, comparing GI, OC II-III, and OC IV groups. Post hoc analysis using Fisher's LSD was applied for group comparisons (*$p < .05$, **$p < .01$, ***$p < .001$, ****$p < .0001$). Dots represent individual data points, the central line in the box indicates the median, and the box edges represent the upper and lower quartiles. Half-violins depict data distributions. Abbreviations: SM, sphingomyelin; Glu-Gly-Arg, glutamyl-glycyl-arginine; PPA, phenylpropionic acid

Potential Microbiota-derived metabolites in Ascites samples

Identification and grading of non-endogenous metabolites with the human microbial metabolome database

The Human Microbial Metabolome Database (MiMeDB) (https://mimedb.org) is a comprehensive multi-omics resource for microbiome research [24]. To explore the potential origins of metabolites that cannot be of

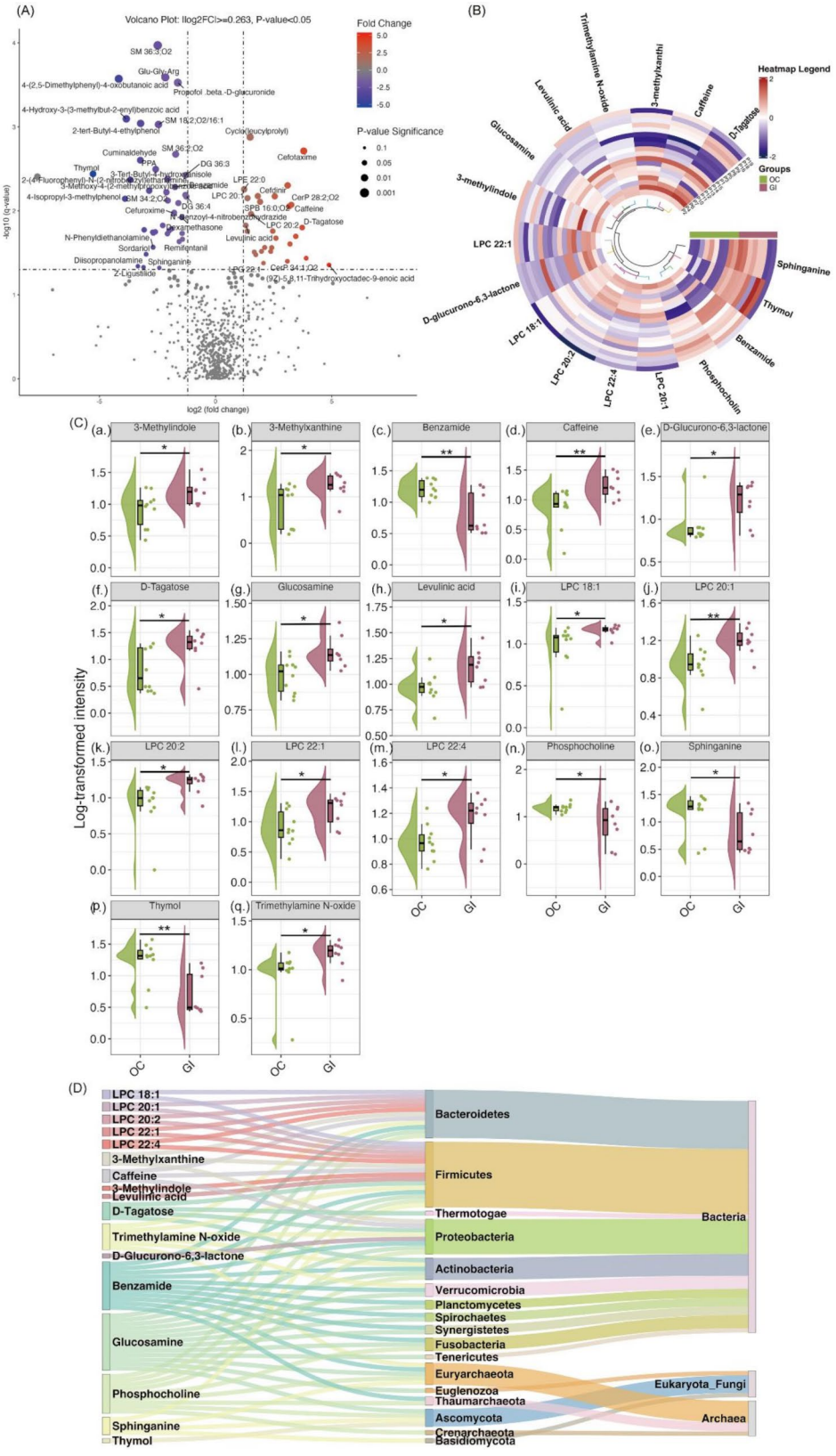

Fig. 2 (See legend on next page.)

(See figure on previous page.)

Fig. 2 Significant Metabolite Changes Between OC and GI Groups. (**A**) Volcano Plot: Red dots indicate metabolites upregulated in the GI group, while blue dots indicate those upregulated in the OC group. Thresholds: fold change ≥ 1.2 and raw *p*-value ≤ 0.05. (**B**) Circular Heatmap: Displays intensity differences of 17 significant microbiota-derived metabolites across 10 OC and 8 GI biological replicates. Analysis used t-tests (raw *p*-value ≤ 0.05, fold change ≥ 1.2), with clustering performed using Ward's hierarchical method and Euclidean distance. (**C**) Raincloud Plots: Show significantly different metabolites between GI and OC groups: (**a**) 3-methylindole, (**b**) 3-methylxanthine, (**c**) benzamide, (**d**) caffeine, (**e**) D-glucurono-6,3-lactone, (**f**) D-tagatose, (**g**) glucosamine, (**h**) levulinic acid, (**i**) LPC 18:1, (**j**) LPC 20:1, (**k**) LPC 20:2, (**l**) LPC 22:1, (**m**) LPC 22:4, (**n**) phosphocholine, (**o**) sphinganine, (**p**) thymol, and (**q**) trimethylamine N-oxide. Unpaired t-tests were applied for comparisons (**p* < .05, ***p* < .01, ****p* < .001, *****p* < .0001). Dots represent individual data points; boxplot lines show medians, quartiles are represented by box edges, and half-violins illustrate data distributions. (**D**) Sankey Plot: Depicts the structure of associated phyla and their respective kingdoms for differentiated microbiota-derived metabolites, highlighting the dominant role of bacteria in the ascites composition of both OC and GI. Abbreviations: LPC, lysophosphatidylcholine; CerP, ceramide phosphate; LPE, lysophosphatidylethanolamine; PE, phosphatidylethanolamine; SPB, sphingoid base; SM, sphingomyelin; PC, phosphatidylcholine; DG, diacylglycerol; Cer, ceramide; DGTS, diacylglyceryl-N, N,N-trimethylhomoserine; PPA, phenylpropionic acid; Glu-Gly-Arg, glutamyl-glycyl-arginine

human-origin and that were identified significant in OC II-III, OC IV, and GI ascites samples, a comparative analysis was first conducted between different stages of OC and between OC and GI. Using the MiMeDB database, significantly increased or decreased metabolites were then examined for their potential origin and relationship to microbiota species.

Differential general and microbiome-derived metabolites in Ascites of OC and GI

Identification of general metabolite changes between OC and GI ascites Based on a fold change (FC) > 1.2 and *p*-value < 0.05, the analysis of normalized intensity data between the OC and GI groups identified 90 significant metabolites out of the 696 measured (Figure S1). Of these, 51 metabolites showed significantly lower intensity, and 39 showed significantly higher intensity in the GI group compared to the OC group. Due to the small sample size of ascites samples, the raw *p*-value was used for this comparison instead of the FDR-adjusted *p*-value (Fig. 2A). We also included the adjusted *p*-values in the Supplementary Table S5.

Sphinganine and phosphocholine were significantly decreased in the GI group compared to the OC group. While LPC 18:1, LPC 20:2, LPC 22:1, and LPC 22:4 lipid compounds were significantly increased in the OC group compared to the GI group.

Identification of microbiota-derived metabolite changes between OC and GI Ascites The MiMeDB database results identified a set of metabolites potentially produced or synthesized by the microbiome, including bacterial species, Eukaryota/Fungi, and Archaea. The associated phyla for the GI vs. OC comparison are listed in Table 2.

Potentially microbiota-derived metabolites significantly increased in GI ascites compared to the OC group included 3-methylindole (a.), 3-methylxanthine (b.), caffeine (d.), D-glucurono-6,3-lactone (e.), D-tagatose (f.), glucosamine (g.), levulinic acid (h.), lysophosphatidylcholine 18:1 (LPC 18:1) (i.), LPC 20:1 (j.), LPC 20:2 (k.), LPC 22:1 (l.), LPC 22:4 (m.), and trimethylamine N-oxide (q.) (Fig. 2C). Conversely, benzamide (c.), phosphocholine (n.), sphinganine (o.), and thymol (p.) were significantly decreased in GI ascites compared to the OC group.

Figure 2B and D illustrate the overall variations in potential microbiota-derived metabolites across the 18 ascites samples from both OC and GI groups. The figures also depict the microbial sources and categories of metabolites that showed increases or decreases in each group, including their associated phyla and respective superkingdoms. In summary, the bacterial kingdom was the predominant source, followed by Archaea, with Eukaryota/Fungi contributing minimally.

Differential general and microbiome-derived metabolites in Ascites of OC stage II-III and stage IV

Identification of general metabolite changes between OC stage II-III and OC stage IV

A comparison between OC II-III (ovarian cancer stage II-III) and OC IV (stage IV) identified 84 significant metabolites out of 649, with 45 showing lower intensities and 39 higher intensities in the OC IV group relative to OC II-III (Fig. 3A). This analysis applied a fold change threshold of 1.2 and a raw *p*-value threshold of 0.05. Due to the limited sample size, raw *p*-values were used instead of FDR-adjusted *p*-values. However, FDR-adjusted *p*-values are provided in Supplementary Table S6 for reference. A heatmap of the 84 significant metabolites was generated to visualize the metabolic differences between OC II-III and OC IV (Figure S2).

Identification of microbiome-derived metabolite changes between OC stage II-III and OC stage IV

The same analysis using the MiMeDB database identified 16 metabolites potentially linked to the microbiome, including those associated with bacterial species, Eukaryota/Fungi, and Archaea. The corresponding phyla for the OC II-III vs. OC IV comparison are provided in Table 3.

The 16 differentiated potential microbiota-derived metabolites between OC II-III and OC IV showed

Table 2 Metabolites potentially derived from the microbiota identified in the comparison between ovarian Cancer (OC) and Gastrointestinal Cancer (GI) groups

Potential Microbiota-derived metabolites (GI vs. OC)	Phylum		
	Bacteria	**Eukaryota/Fungi**	**Archaea**
Thymol	/	Ascomycota	/
Benzamide	Proteobacteria, Verrucomicrobia, Synergistetes, Firmicutes, Actinobacteria, Bacteroidetes, Spirochaetes, Fusobacteria, Planctomycetes	/	Thaumarchaeota, Euryarchaeota,
LPC 20:1	Bacteroidetes, Firmicutes	/	/
Caffeine	Bacteroidetes, Firmicutes, Proteobacteria	/	/
Glucosamine	Actinobacteria, Bacteroidetes, Firmicutes, Proteobacteria, Verrucomicrobia, Spirochaetes, Fusobacteria, Synergistetes, Tenericutes, Planctomycetes	Ascomycota, Euglenozoa,	Euryarchaeota
LPC 20:2	Bacteroidetes, Firmicutes	/	/
Levulinic acid	Firmicutes	/	/
D-Tagatose	Firmicutes, Proteobacteria, Thermotogae, Actinobacteria	/	/
LPC 22:4	Bacteroidetes, Firmicutes	/	/
3-Methylxanthine	Bacteroidetes, Firmicutes, Proteobacteria	/	/
D-Glucurono-6,3-lactone	Proteobacteria	/	/
Phosphocholine	Bacteroidetes, Firmicutes, Proteobacteria, Actinobacteria, Fusobacteria	Ascomycota	Thaumarchaeota, Euryarchaeota, Crenarchaeota
Trimethylamine N-oxide	Firmicutes, Proteobacteria, Actinobacteria, Verrucomicrobia, Bacteroidetes	/	Euryarchaeota
3-Methylindole	Firmicutes	/	/
LPC 22:1	Bacteroidetes, Firmicutes	/	/
LPC 18:1	Bacteroidetes, Firmicutes	/	/
Sphinganine	Firmicutes	Ascomycota, Basidiomycota	Euryarchaeota

Note. This table lists metabolites identified as potentially derived from the microbiota, based on the MiMeDB database. The corresponding phyla responsible for producing or synthesizing these compounds are included

significant changes. Specifically, 1-methylhistidine (a.), 3-hydroxyanthranilic acid (b.), 4-pyridoxic acid (c.), biliverdin (e.), butyryl-L-carnitine (f.), hydroxypropionic acid (g.), indole (h.), lysophosphatidylinositol 18:1 (LPI 18:1) (i.), mevalonic acid (j.), N-acetyl-L-phenylalanine (k.), and nudifloramide (m.) were elevated in OC IV ascites samples compared to OC II-III. On the other hand, benzyl alcohol (d.), naringenin (l.), o-cresol (n.), octadecanedioic acid (o.), and phenol (p.) were significantly reduced in the OC IV group relative to OC II-III. These changes suggest distinct metabolic shifts between ovarian cancer stages II-III and IV, potentially reflecting the progression of the disease. The corresponding metabolite alterations are visualized in Fig. 3C.

The broad metabolic variations in potential microbiota-derived metabolites across the 7 OC II-III and 3 OC IV ascites samples, highlighting distinct shifts between early and advanced stages of ovarian cancer (Fig. 3B). The microbial sources and categories of the metabolites that exhibited alterations between the OC II-III and OC IV groups, including their associated phyla and respective superkingdoms (Fig. 3D). Bacteria emerged as the primary source of these metabolites, followed by Eukaryota/Fungi, with Archaea contributing the least. These findings suggest that the microbiota's involvement in ovarian cancer progression may stem from a diverse array of microbial species, each potentially playing a specific role in influencing the tumor microenvironment and disease progression.

Correlations between potentially microbiota-derived metabolites and cytokines/chemokines in Ascites

Ovarian Cancer vs. Gastrointestinal Cancer

To investigate potential interactions between microbiota-derived metabolites and cytokines, a correlation analysis was performed between individual metabolites from the OC vs. GI comparison and cytokine levels (Fig. 4A). Due to the small sample size of ascites samples, the raw *p*-value was used for this comparison instead of the FDR-adjusted *p*-value. The FDR-adjusted *p*-value information is included in Supplementary Table S7. The results revealed several significant correlations amongst metabolites and cytokines/chemokines. Cytokine IL-23 showed a positive correlation with D-glucurono-6,3-lactone and a negative correlation with trimethylamine N-oxide. IL-18 was negatively correlated with caffeine. IL-10 demonstrated significant positive correlations with glucosamine, D-tagatose, trimethylamine N-oxide, caffeine, LPC 22:4, and LPC 20:1, while showing negative correlations with benzamide and thymol. TNF-α positively correlated with D-glucurono-6,3-lactone. IFN-γ was negatively correlated with levulinic acid and trimethylamine N-oxide,

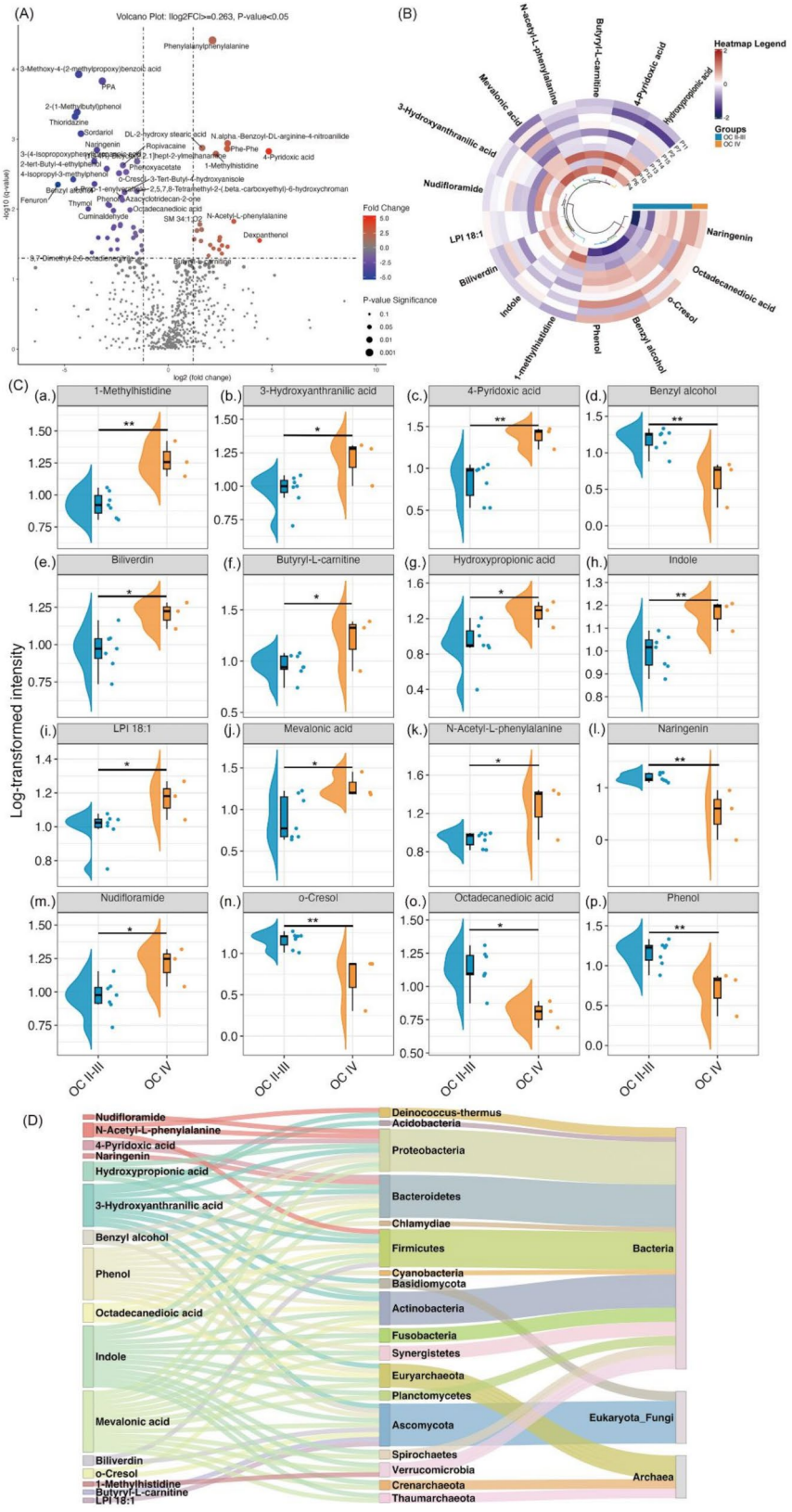

Fig. 3 (See legend on next page.)

(See figure on previous page.)

Fig. 3 Significant Metabolite Changes Between OC II-III and OC IV Groups. (**A**) Volcano Plot: Red dots represent metabolites upregulated in OC IV, while blue dots represent those upregulated in OC II-III. Thresholds: fold change ≥ 1.2 and raw *p*-value ≤ 0.05. (**B**) Circular Heatmap: Displays intensity variations of 16 significant microbiota-derived metabolites across 7 OC II-III and 3 OC IV biological replicates. Analysis was performed using t-tests (raw *p*-value ≤ 0.05, fold change ≥ 1.2), with clustering based on Ward's hierarchical method and Euclidean distance. (**C**) Raincloud Plots: Show significantly different metabolites between OC II-III and OC IV groups: (**a**) 1-methylhistidine, (**b**) 3-hydroxyanthranilic acid, (**c**) 4-pyridoxic acid, (**d**) benzyl alcohol, (**e**) biliverdin, (**f**) butyryl-L-carnitine, (**g**) hydroxypropionic acid, (**h**) indole, (**i**) LPI 18:1, (**j**) mevalonic acid, (**k**) N-acetyl-L-phenylalanine, (**l**) naringenin, (**m**) nudifloramide, (**n**) o-cresol, (**o**) octadecanedioic acid, and (**p**) phenol. Unpaired t-tests were applied for comparisons (**p* <.05, ***p* <.01, ****p* <.001, *****p* <.0001). Dots represent individual data points; the boxplot's central line indicates the median, with quartiles represented by box edges, and half-violins illustrating data distributions. (**D**) Sankey Plot: Depicts microbial phyla and their respective superkingdoms associated with altered metabolites, emphasizing the dominant role of bacteria and their interactions with Eukaryota/Fungi and Archaea in the ascites of advanced ovarian cancer. Abbreviations: LPC, lysophosphatidylcholine; MG, monoacylglycerol; Phe-Phe, phenylalanine-phenylalanine; Phe-Leu, phenylalanine-leucine; CerP, ceramide phosphate; SM, sphingomyelin; LPI, lysophosphatidylinositol; PC, phosphatidylcholine; PPA, phenylpropionic acid; PE, phosphatidylethanolamine

while IFN-α2 showed a positive correlation with D-glucurono-6,3-lactone. Chemokine MCP-1 was negatively correlated with D-tagatose.

Ovarian Cancer stage II-III vs. stages IV

A similar correlation analysis was performed between microbiota-derived metabolites from the OC II-III vs. OC IV comparison and cytokine levels (Fig. 4B). Given the small sample size, raw *p*-values were used instead of FDR-adjusted *p*-values. Supplementary Table S8 presents the FDR-adjusted *p*-values. The analysis identified significant correlations. Chemokine IL-8 showed negative correlations with 3-hydroxyanthranilic acid and nudifloramide. MCP-1 was positively correlated with benzyl alcohol, naringenin, o-cresol, octadecanedioic acid, and phenol, while negatively correlated with 1-methylhistidine, 4-pyridoxic acid, and mevalonic acid. Cytokine IL-6 demonstrated negative correlations with butyryl-L-carnitine, indole, nudifloramide and N-acetyl-L-phenylalanine. IL-1β exhibited positive correlations with 1-methylhistidine, 4-pyridoxic acid, LPI 18:1 and mevalonic acid, and negative correlations with benzyl alcohol, naringenin, o-cresol, octadecanedioic acid, and phenol.

Discussion

Malignant ascites forms due to a combination of increased fluid production and reduced lymphatic absorption [25, 26]. Normally, the peritoneum absorbs excess fluid through lymphatic channels, but in malignancy, the tumor's growth and invasion disrupt these processes. Tumor-induced neovascularization [7], driven by vascular endothelial growth factor (VEGF), increases vascular permeability, leading to fluid leakage into the abdominal cavity [8, 27]. Matrix metalloproteinases (MMPs) also degrade tissue barriers, further promoting fluid accumulation [28, 29]. In addition, hormonal changes activate the renin-angiotensin-aldosterone system, causing sodium and fluid retention [6].

Emerging research suggests the microbiota may influence ascites development. Disruption of gut bacteria has been linked to inflammation, altered immune responses, and cancer progression [30–32]. In malignancies, an imbalanced gut microbiota can impair the intestinal barrier, increasing permeability and allowing bacterial translocation [33, 34]. This worsens inflammation and fluid retention, creating a cycle that perpetuates ascites formation. The role of gut microbiota in modulating immune and metabolic pathways presents a potential area for further exploration in managing malignant ascites [35].

LC-MS based metabolomic profiles of OC stages II-III, IV and GI Ascites samples

Metabolic analysis of ascites from the OC II-III, OC IV, and GI groups revealed that OC IV shares more similarities with the GI group, while OC II-III is distinctly different from both. The GI group included patients with various cancer origins and histological subtypes; notably, two patients had received neoadjuvant therapy, and one patient was male. Despite this heterogeneity, we included all available GI cases to provide a general overview. Our aim was to capture the broader metabolic landscape of advanced disease, as OC at stage IV exhibits features increasingly similar to those observed in GI cancers with peritoneal metastasis. This pattern aligns with the progression of ovarian cancer, where advanced stages involve cancer cells detaching from the primary tumor, surviving in the peritoneal fluid, and spreading to organs such as the liver, lungs, spleen, intestines, and lymph nodes [36–38].

One metabolite, phenylalanylphenylalanine, a dipeptide of two phenylalanine molecules, was found at higher levels in OC IV. Elevated phenylalanine levels and altered phenylalanine-to-tyrosine ratios have been associated with inflammatory conditions, including cancer [39]. Phenylalanine metabolism also influences T-cell function, regulate T-cell proliferation and activation and affecting the following immune response [39]. This suggests that higher levels of phenylalanylphenylalanine could be linked to more advanced cancer stages. Similarly, SM 36:3;O2, a sphingomyelin, was significantly elevated in OC IV. Increased sphingomyelin levels have been linked to cancer development, with altered sphingomyelin metabolism observed in metastatic tumor cells and various cancers [40–42]. These changes in sphingomyelin

Table 3 Metabolites potentially derived from the microbiota identified in the comparison between ovarian Cancer stage II-III and stage IV

Potential Microbiota-derived metabolites (GI vs. OC)	Phylum		
	Bacteria	**Eukaryota/Fungi**	**Archaea**
Naringenin	Bacteroidetes	/	/
4-Pyridoxic acid	Bacteroidetes, Proteobacteria	/	/
1-Methylhistidine	Verrucomicrobia	/	/
o-Cresol	Actinobacteria	Ascomycota	/
Benzyl alcohol	Proteobacteria, Bacteroidetes	Ascomycota,	/
Indole	Bacteroidetes, Firmicutes, Fusobacteria, Proteobacteria, Spirochaetes, Verrucomicrobia, Actinobacteria, Synergistetes, Planctomycetes	Ascomycota	Euryarchaeota, Thaumarchaeota, Crenarchaeota
Phenol	Bacteroidetes, Firmicutes, Fusobacteria, Proteobacteria, Actinobacteria, Synergistetes, Chlamydiae, Cyanobacteria	Ascomycota, Basidiomycota	Euryarchaeota
Octadecanedioic acid	Bacteroidetes, Firmicutes, Actinobacteria	/	Euryarchaeota
N-Acetyl-L-phenylalanine	Firmicutes, Proteobacteria, Deinococcus-thermus	/	/
Biliverdin	Firmicutes	Ascomycota	/
Nudifloramide	Proteobacteria	/	/
3-Hydroxyanthranilic acid	Proteobacteria, Firmicutes, Actinobacteria, Bacteroidetes, Deinococcus-thermus, Acidobacteria	Ascomycota, Basidiomycota	Euryarchaeota,
Hydroxypropionic acid	Proteobacteria, Firmicutes, Actinobacteria, Bacteroidetes	/	/
LPI 18:1	/	Ascomycota	/
Mevalonic acid	Verrucomicrobia, Firmicutes, Actinobacteria, Proteobacteria, Bacteroidetes, Spirochaetes, Fusobacteria, Synergistetes, Planctomycetes	Ascomycota	Euryarchaeota, Thaumarchaeota, Crenarchaeota,
Butyryl-L-carnitine	/	Ascomycota	/

Note. This table lists metabolites identified as potentially originating from the microbiota, based on the MiMeDB database. The associated phyla known to produce or synthesize these metabolites are also indicated

metabolism, including higher synthesis and reduced breakdown, contribute to disrupted lipid balance, promoting cancer growth, particularly in ovarian and breast cancers [43, 44]. The higher levels of sphingomyelin in ascites may, therefore, reflect more aggressive tumor behavior and advanced disease.

LC-MS analysis also detected a wide range of metabolites in the ascites samples, many of which are not directly related to human metabolism. Several of the significantly different compounds were identified as exogenous substances, including drugs, food-derived compounds, plant oil-derived, and anesthetics. These findings highlight the complexity of ascites as a mixture of both endogenous and exogenous compounds. The presence of these exogenous compounds can be explained by several factors. Medications such as chemotherapeutics, anesthetics, and pain management drugs are commonly used in ovarian cancer treatment, and residual traces can accumulate in bodily fluids [45]. Additionally, diet and environmental exposure significantly influence an individual's metabolic profile [46, 47]. Plant-derived compounds or food additives can enter the bloodstream and appear in ascites, particularly in patients undergoing systemic changes due to disease or treatment [48]. This suggests that ascites is influenced by both internal metabolic processes and external factors, complicating the interpretation of LC-MS data.

Potential microbiota-derived metabolomic features in malignant Ascites samples

Through MiMeDB analysis, we identified 17 microbiota-derived metabolites in the OC vs. GI comparison and 16 in the OC II-III vs. OC IV comparison. Both sets revealed a predominance of bacterial-origin metabolites in malignant ascites, consistent with the human gut microbiota profile [49]. While the proportions of Archaea and Eukaryota/Fungi-derived metabolites showed slight differences between the two sets, the findings align with studies highlighting the role of gut microbiota in carcinogenesis, immune surveillance, and responses to immunotherapy [50–52].

In OC patients, continuous immune checkpoint blockade (ICB) therapy with poly (ADP-ribose) polymerase inhibitors (PARPi) has demonstrated efficacy in prolonging progression-free and overall survival [53–56]. For GI cancers, ICB strategies vary by tumor origin. Immunotherapy is now standard in first-line treatment for advanced colorectal cancer with high microsatellite instability [57–60]. Additionally, in advanced gastric cancer, combining immunotherapy with chemotherapy or with HER2-targeted therapy has shown significant and lasting survival benefits in HER2-positive patients [61–64].

Despite advances in immunotherapy, a significant proportion of patients exhibit primary or acquired resistance to treatment [65, 66]. Additionally,

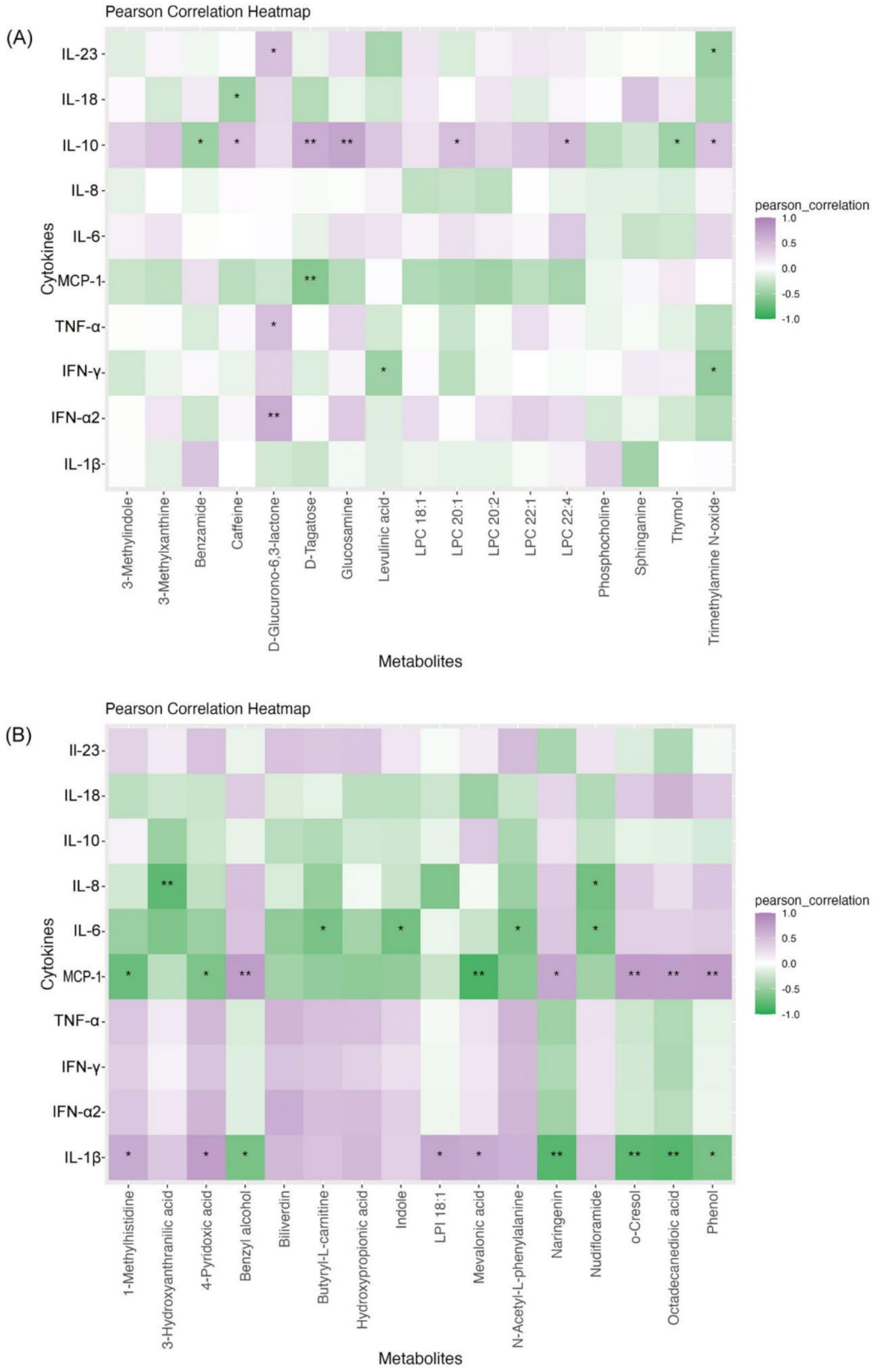

Fig. 4 Heatmap of Correlations Between Potential Microbiota-derived Metabolites and Flow Cytometry Cytokines/Chemokines. (**A**) OC vs. GI, (**B**) OC II-III vs. OC IV, the heatmap illustrates the correlations between microbiota-derived metabolites and cytokines measured by flow cytometry. A single asterisk (*) indicates a significant correlation ($p < 0.05$), while a double asterisk (**) represents a highly significant correlation ($p < 0.01$). Correlations were calculated using Pearson method for normally distributed data. Abbreviations: LPI, Lysophosphatidylinositol

immunotherapy-related adverse reactions pose a clinical challenge, particularly with the expanded use of combination therapies and multi-agent immunotherapy [67–74]. To address these challenges, studies have identified host-associated genomic and molecular biomarkers predictive of immunotherapy response [75–77]. Emerging evidence also implicates the gut microbiome, particularly specific microbial taxa, in modulating immune checkpoint blockade (ICB) efficacy [78].

Research suggests that gut microbiome composition may be both predictive and prognostic of therapeutic response to ICB, highlighting its potential as a biomarker [78]. These insights have driven the development of microbiome-targeted strategies aimed at enhancing treatment efficacy and minimizing adverse effects by modulating the patient's gut microbiota [79, 80].

The microbiota-derived metabolites identified in ascites contribute significantly to the tumor microenvironment. This study revealed distinct microbiota profiles across ovarian cancer stages and gastrointestinal cancers, highlighting the importance of larger sample sizes and advanced tools like 16 S rRNA sequencing to enhance our understanding. Further research is needed to explore how these microbial profiles correlate with immunotherapy side effects, tumor reduction efficacy, and clinical outcomes, providing insight into their role in ascites formation and cancer progression.

Emerging interventions, such as fecal microbiota transplants (FMT), prebiotics, probiotics, antibiotics, and dietary modifications, show promise in modulating the gut microbiome [81–83]. Characterizing microbiota and its systemic effects will be key to identifying actionable targets for future therapeutic interventions and clinical assessment.

Microbiota-Derived metabolomic profiles in Ascites from OC and GI

Several bacterial-derived metabolites identified in the OC vs. GI comparison are associated with immune-metabolic pathways and may affect immune responses in ovarian and gastrointestinal cancers. Lysophosphatidylcholines (LPCs), known pro-inflammatory lipids [84], are influenced by microbial taxa such as *Bacteroidetes* and *Firmicutes* [85]. Bacteroidetes contribute to lipid absorption and metabolism, while firmicutes play a role in immune modulation through lipid pathways [86–88]. In cancer, LPCs contribute to inflammation, tumor growth, and immune evasion [89]. Dysbiosis between these taxa may alter LPC levels and functions, impacting cancer progression, immune response, and gut health. The presence of LPCs (LPC 18:1, LPC 20:1, LPC 20:2, LPC 22:1, LPC 22:4) and sphingolipids (sphinganine) indicates significant involvement in membrane turnover and lipid signaling, both commonly disrupted in cancer [90–92].

Additionally, metabolites such as 3-methylindole and trimethylamine N-oxide suggest shifts in gut microbiota metabolism that may impact cancer progression or immune function [93, 94]. Detoxification metabolites, like D-glucurono-6,3-lactone, reflect an active response to cellular stress, arising from cancer or external treatments such as chemotherapy [95]. This aligns with the clinical profiles of the eight GI patients, two of whom underwent neoadjuvant chemotherapy.

Differential potential microbiota-derived metabolites in ascites: OC II-III vs. OC IV

In the comparison between OC stages II-III and IV, several metabolites reflect metabolic changes, immune modulation, and inflammatory responses typical of the tumor microenvironment, particularly in advanced stages. Metabolites such as mevalonic acid, butyryl-L-carnitine, and LPI 18:1 suggest shifts in lipid metabolism, likely driven by heightened energy demands, membrane synthesis, and signaling activity in ovarian cancer cells [96, 97]. Additionally, 3-hydroxyanthranilic acid, indole, and naringenin indicate the presence of immune-modulating and inflammatory metabolites, potentially promoting immune evasion and supporting a pro-inflammatory environment in advanced cancer [98–101].

LPI 18:1, a bioactive lipid involved in cell signaling, is linked to tumor growth, migration, and immune suppression, and its levels may be influenced by gut microbiota, especially in cases of dysbiosis [96, 97]. Indole, a microbial byproduct of tryptophan degradation, can affect immune responses and inflammation, potentially aiding immune evasion in cancer [100]. These findings underscore the interaction between microbial metabolites and the tumor microenvironment, highlighting the gut-tumor axis's role in cancer progression and suggesting therapeutic strategies that target the microbiota to improve outcomes.

Naringenin, known for its anti-inflammatory, antioxidant, and anticancer effects [101–103], was elevated in OC II-III compared to OC IV. It modulates inflammation by suppressing cytokine production and enhancing cytokine degradation [104], while also regulating cell growth, apoptosis, and metastasis [105, 106]. Its higher levels in OC II-III suggest naringenin may help regulate immune responses and inhibit cancer progression in early stages, with reduced activity as the disease advances.

Interactions between microbiota-derived metabolites and cytokines/chemokines

To investigate how microbiota-derived metabolites interact with the immune landscape in cancer progression, we conducted correlation analyses between these metabolites and cytokines in OC vs. GI and OC stage II-III vs. IV comparisons. The anti-inflammatory cytokine IL-10

showed multiple positive correlations with metabolites such as glucosamine, D-tagatose, TMAO, caffeine, LPC 22:4, and LPC 20:1, suggesting these metabolites may contribute to immune suppression in the tumor microenvironment. This immune tolerance could facilitate tumor evasion from immune surveillance. Conversely, IL-10 was negatively correlated with benzamide and thymol, illustrating how different metabolites exert opposing influences on cytokine regulation. Notably, IL-10 in ascites has been associated with both the migration of ovarian cancer cells [107] and, in some cases, longer survival in patients receiving cell-free and concentrated ascites reinfusion therapy (CART) [108].

MCP-1 chemokine that recruits monocytes and macrophages to the tumor site, was positively correlated with metabolites like benzyl alcohol, naringenin, o-cresol, octadecanedioic acid, and phenol, potentially promoting immune cell recruitment and inflammation. In contrast, 1-methylhistidine, 4-pyridoxic acid, and mevalonic acid were negatively correlated with MCP-1 chemokine, potentially reducing immune cell recruitment. This dual influence suggests a complex delicate balance of pro- and anti-inflammatory signals in advanced ovarian cancer, where shifts in metabolite levels may influence MCP-1 bioactivity. Additionally, MCP-1's positive association with infertility in endometriosis patients highlights its role in inflammatory immune reactions within the peritoneal cavity [109–111].

Together, these findings illustrate an intricate network of interactions between metabolites and cytokines/chemokines that likely impact cancer progression, immune evasion, and patient outcomes. Observed stage-dependent differences underscore the influence of metabolic shifts on immune responses within the tumor microenvironment. The balance of pro- and anti-inflammatory metabolites, in particular, may play a critical role in shaping this environment.

However, the small sample size in this study may increase the risk of type I statistical errors, potentially leading to false-positive findings. This is particularly relevant for the GI group, which included only 8 samples and exhibited substantial heterogeneity in cancer origin and histological subtype. Additionally, two patients had received neoadjuvant therapy, and one patient was male. We also did not include BMI as a parameter, and we would like to clarify this decision. In patients with malignant ascites, body weight does not accurately reflect true body mass due to the accumulation of large fluid volumes. This can distort BMI calculations and introduce further confounding into the analysis. While we initially considered including BMI, we ultimately excluded it to avoid misinterpretation. Future approaches that estimate or approximate dry body weight may offer more meaningful insights.

Other clinical variables—such as prior chemotherapy, antibiotic use, diet, medications, and infection status—were not controlled for in this exploratory study but are important potential confounders that should be considered in future research.

This study represents an initial step toward characterizing the metabolic landscape of ascites in cancer. Validation in larger, more homogeneous cohorts or through multi-center collaborations is strongly warranted. Expanding the GI group in particular would allow for meaningful stratification by cancer origin and histological subtype, thereby improving the precision and interpretability of the results.

Additionally, the detection and interpretation of bacterial metabolites could be enhanced by integrating LC-MS with targeted microbial profiling methods such as 16 S rRNA sequencing. This combined approach would enable more accurate characterization of the microbiome's contribution to the ascitic metabolome and provide deeper insights into its role in cancer progression.

We summarized our findings, especially the microbiota-derived metabolomic differentiation in ascites samples from OC II-III and OC IV (Fig. 5).

Conclusion

This study utilized novel trapped ion mobility spectrometry time of flight (timsTOF) mass spectrometry (MS) to profile metabolites in malignant ascites samples, comparing gastrointestinal cancers and different stages ovarian cancers. Both reversed-phase and hydrophilic interaction liquid chromatography were employed to ensure comprehensive separation of non-polar and polar metabolites. Key findings revealed distinct potential microbiota-derived metabolic changes in OC versus GI cancers and across ovarian cancer stages, particularly involving lipid metabolism, with significant alterations in sphingolipid and phospholipid pathways. Additionally, potential microbiota-derived metabolites were identified and correlated with cytokine and chemokine levels, indicating a possible interaction between microbiota and the immune response in ovarian and gastrointestinal cancers. These findings show the presence of microbiota-derived metabolites in malignant ascites and contribute as first step to a better understanding of the interplay between microbiota and intestinal malignancies. Future studies upon malignant ascites shall follow, assessing the exact impact of individual microbial metabolites upon the tumor microenvironment to improve patient care and support the success of novel cancer therapies.

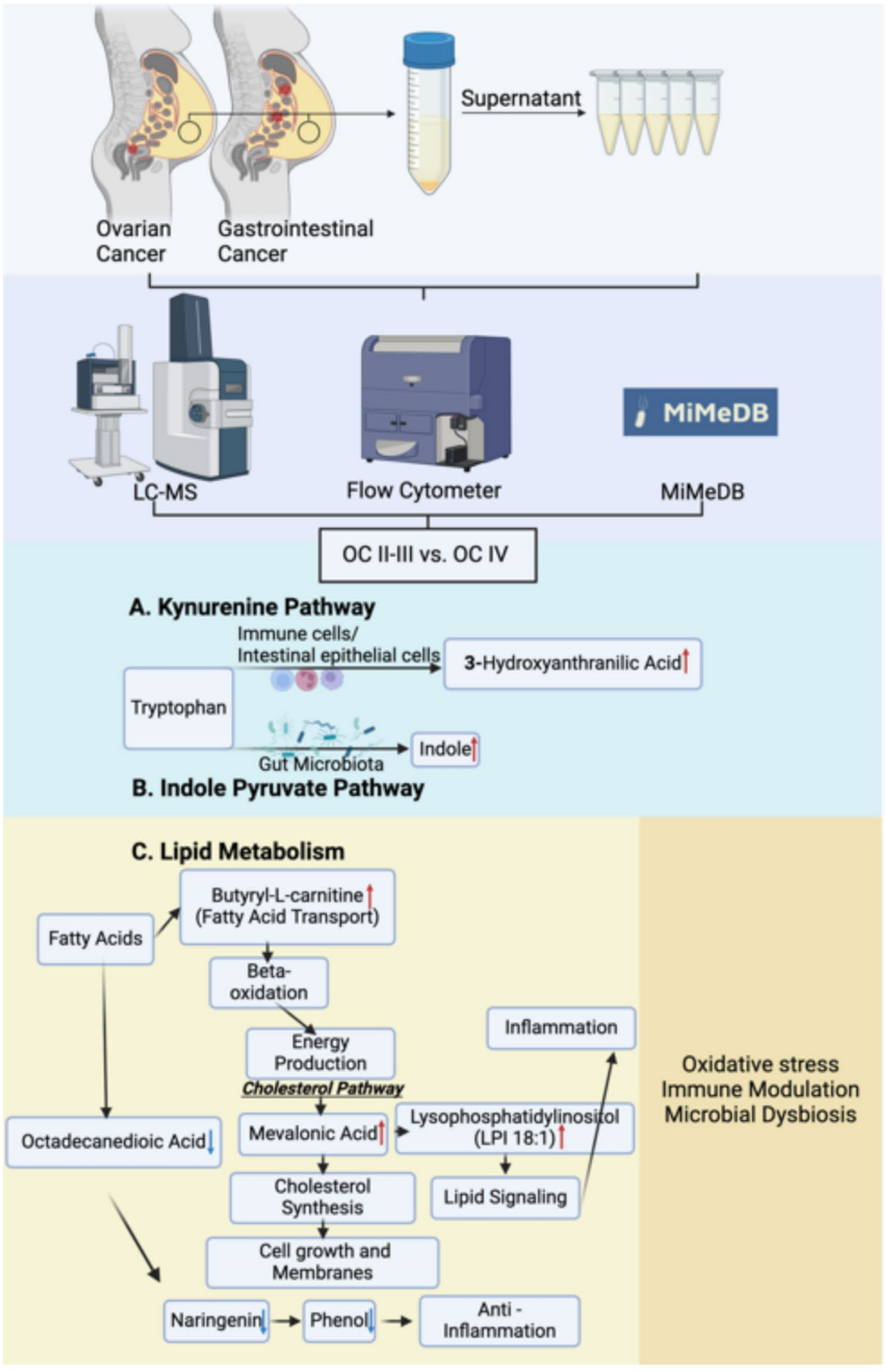

Fig. 5 Graphical abstract to present microbiota-derived metabolomic differentiation in ascites samples from OC II-III and OC IV. Red and blue arrow means increase and decrease in OC IV ascites compare to OC II-III

Abbreviations

9-OAHSA	9-Oxoheptadecanoic Acid
ADENOCA	Subtype unknown adenocarcinoma
Ala Glu Ile Lys	Alanine-Glutamic Acid-Isoleucine-Lysine peptide
CCS	Collision cross section
Cer 42:2;O2	Ceramide with 42 carbons, 2 double bonds, and 2 oxygen atoms
CerP 28:1;O2	Ceramide Phosphate with 28 carbons, 1 double bond, and 2 oxygen atoms
CerP 32:0;O2	Ceramide Phosphate with 32 carbons and no double bonds
Co	Control
DG 34:3	Diacylglycerol with 34 carbons and 3 double bonds
GC	Gas chromatography

Glu-Gly-Arg	Glutamic Acid-Glycine-Arginine peptide
HGSC	High-grade serous carcinoma
HILIC	Hydrophilic interaction liquid chromatography
HMDB	Human Metabolome Database
HPLC	High-performance liquid chromatography
IL-10	Interleukin 10
IL-18	Interleukin 18
IL-6	Interleukin 6
IL-8	Interleukin 8
LC	Liquid chromatography
Leu Leu Val Val Ala	Leucine-Leucine-Valine-Valine-Alanine peptide
LPC	Lysophosphatidylcholine
LPC 22:0	Lysophosphatidylcholine with a 22-carbon saturated fatty acid
LPC 22:1	Lysophosphatidylcholine with a 22-carbon monounsaturated fatty acid
LPC 22:2	Lysophosphatidylcholine with a 22-carbon polyunsaturated fatty acid
LPC 22:3	Lysophosphatidylcholine with a 22-carbon fatty acid and 3 double bonds
LPE	Lysophosphatidylethanolamine
LPE O-16:0	Lysophosphatidylethanolamine with a 16-carbon saturated fatty acid and an ether linkage
LPE O-16:1	Lysophosphatidylethanolamine with a 16-carbon fatty acid and 1 double bond, with an ether linkage
LPE O-16:2	Lysophosphatidylethanolamine with a 16-carbon fatty acid and 2 double bonds, with an ether linkage
LPE O-18:2	Lysophosphatidylethanolamine with an 18-carbon fatty acid and 2 double bonds, with an ether linkage
LPE O-18:3	Lysophosphatidylethanolamine with an 18-carbon fatty acid and 3 double bonds, with an ether linkage
LPS 18:1	Lysophosphatidylserine with an 18-carbon fatty acid and 1 double bond
LPS 20:0	Lysophosphatidylserine with a 20-carbon saturated fatty acid
MCP-1	Monocyte chemoattractant protein-1
MG 18:2	Monoglyceride with an 18-carbon fatty acid and 2 double bonds
MQ	MilliQ water
MS	Mass spectrometry
NAFLD	Non-alcoholic fatty liver disease
NIST	National Institute of Standards and Technology
NMR	Nuclear magnetic resonance
OC III	Ovarian cancer stage III
OC IV	Ovarian cancer stage IV
PASEF	Parallel Accumulation–Serial Fragmentation
PC	Phosphatidylcholine
PC O-38:5	Phosphatidylcholine with 38 carbons, 5 double bonds, and an ether linkage
PE	Phosphatidylethanolamine
PE 38:1	Phosphatidylethanolamine with 38 carbons and 1 double bond
PE O-34:3	Phosphatidylethanolamine with 34 carbons, 3 double bonds, and an ether linkage
PE O-36:5	Phosphatidylethanolamine with 36 carbons, 5 double bonds, and an ether linkage
PE O-38:5	Phosphatidylethanolamine with 38 carbons, 5 double bonds, and an ether linkage
PE O-38:6	Phosphatidylethanolamine with 38 carbons, 6 double bonds, and an ether linkage
PG 18:1_18:2	Phosphatidylglycerol with one 18:1 and one 18:2 fatty acid chains
Phe Leu	Phenylalanine-Leucine peptide
Phe-Phe	Phenylalanine-Phenylalanine dipeptide
PPA	Phenylpropionic Acid
PQN	Probabilistic quotient normalization
QTOF	Quadrupole Time-of-Flight
RNS	Nitrogen species
ROS	Reactive oxygen species
RPLC	Reversed-phase liquid chromatography
SBP	Spontaneous bacterial peritonitis
SM 30:1;O2	Sphingomyelin with 30 carbons, 1 double bond, and 2 oxygen atoms
SM 30:2;O2	Sphingomyelin with 30 carbons, 2 double bonds, and 2 oxygen atoms
SM 32:1;O2	Sphingomyelin with 32 carbons, 1 double bond, and 2 oxygen atoms
SM 32:2;O2	Sphingomyelin with 32 carbons, 2 double bonds, and 2 oxygen atoms
SM 34:1;O2	Sphingomyelin with 34 carbons, 1 double bond, and 2 oxygen atoms
SM 34:1;O2	Sphingomyelin with 34 carbons, 1 double bond, and 2 oxygen atoms
SM 34:2;O2	Sphingomyelin with 34 carbons, 2 double bonds, and 2 oxygen atoms
SM 36:3;O2	Sphingomyelin with 36 carbons, 3 double bonds, and 2 oxygen atoms
SM 44:6;O2	Sphingomyelin with 44 carbons, 6 double bonds, and 2 oxygen atoms
TAM	Tumor-associated macrophage
TIMS	Trapped Ion Mobility Spectrometry
VIP-HESI	Vacuum insulated probe heated electrospray ionization

Supplementary Information

The online version contains supplementary material available at https://doi.org/10.1186/s40170-025-00391-5.

Supplementary Material 1

Acknowledgements

We thank all patients who consented to participate in this study. We thank Giorgi Nadiradze, Arianna Castagna, Marc A. Reymond and Silvia Wagner form the Department of General, Visceral and Transplant Surgery, University Hospital Tübingen, Germany, for the samples collection work.

Author contributions

Conception: C.T., S.D., N.B., S.K. Data acquisition: W.K., Y.S., G.B., Q.Y., K.C. Data analysis: S.D., W.K., Y.S., C.T. Interpretation of data: C.T., S.D., W.K. Figure preparation: S.D.Manuscript draft: S.D. Manuscript editing: S.D., W.K., G.B., Y.S., L.M., S.K., N.B., J.S., C.T. All authors have approved the submitted version. S.D., W.K., K.C, Q.Y., Y.S., G.B., S.K., N.B., L.M., J.S., C.T.

Funding

Open Access funding enabled and organized by Projekt DEAL.
This work was supported by Bruker Switzerland AG by free provision of MetaboScape® software upgrades.

Data availability

The data supporting this study are available from the corresponding author upon reasonable request.

Declarations

Ethical approval and consent to participate

Written informed consent was obtained from each patient prior to obtaining the sample to use for research purposes. Analyses of ascites samples was approved by the Ethics Committee, University of Tübingen, Germany (Ref. Nr. 696/2016BO2 and 117/2020BO1).

Conflict of interest

AG. S.D., W.K., K.C, Q.Y., Y.S., G.B., S.K., N.B., L.M.and J.S. declare that they have no competing interests. CT reports a research grant by Bruker Switzerland AG.

Author details

[1]Department of Preclinical Imaging and Radiopharmacy, Werner Siemens Imaging Center, University Hospital Tübingen, Tübingen, Germany
[2]Cluster of Excellence iFIT (EXC 2180) "Image Guided and Functionally Instructed Tumor Therapies", University of Tübingen, Tübingen, Germany
[3]Core Facility Metabolomics, Faculty of Medicine, University of Tübingen, Tübingen, Germany

[4]M3 Research Center for Microbiome, Metabolome and Malignome, Faculty of Medicine, University of Tübingen, Tübingen, Germany
[5]Institute of Medical Genetics and Applied Genomics, University of Tübingen, Tübingen, Germany
[6]Department of Obstetrics and Gynecology, Diak Klinikum, Schäbisch Hall, Germany
[7]Cluster of Excellence CMFI (EXC 2124) "Controlling Microbes to Fight Infections", Eberhard Karls University of Tübingen, Tübingen, Germany
[8]Department of Internal Medicine I, Faculty of Medicine, University of Tübingen, Tübingen, Germany
[9]Department of Physiology and Pharmacology, Snyder Institute for Chronic Diseases, Cumming School of Medicine, University of Calgary, Calgary, AB T2N 4N1, Canada

Received: 5 December 2024 / Accepted: 26 April 2025
Published online: 13 May 2025

References

1. Momenimovahed Z, Tiznobaik A, Taheri S, Salehiniya H. Ovarian cancer in the world: epidemiology and risk factors. Int J Womens Health. 2019;11:287–99.
2. Patni R. Screening for ovarian cancer: an update. J Midlife Health. 2019;10(1):3–5.
3. Webb PM, Jordan SJ. Global epidemiology of epithelial ovarian cancer. Nat Rev Clin Oncol. 2024;21(5):389–400.
4. Garrison RN, Kaelin LD, Galloway RH, Heuser LS. Malignant ascites. Clinical and experimental observations. Ann Surg. 1986;203(6):644–51.
5. Runyon BA. Care of patients with Ascites. N Engl J Med. 1994;330(5):337–42.
6. Smith EM, Jayson GC. The current and future management of malignant Ascites. Clin Oncol (R Coll Radiol). 2003;15(2):59–72.
7. Adam RA, Adam YG. Malignant ascites: past, present, and future. J Am Coll Surg. 2004;198(6):999–1011.
8. Zebrowski BK, Liu W, Ramirez K, Akagi Y, Mills GB, Ellis LM. Markedly elevated levels of vascular endothelial growth factor in malignant Ascites. Ann Surg Oncol. 1999;6(4):373–8.
9. Cavazzoni E, Bugiantella W, Graziosi L, Franceschini MS, Donini A. Malignant ascites: pathophysiology and treatment. Int J Clin Oncol. 2013;18(1):1–9.
10. Mizoguchi R, Karashima S, Miyajima Y, Ogura K, Kometani M, Aono D, et al. Impact of gut Microbiome on the renin-aldosterone system: Shikamachi super preventive health examination results. Hypertens Res. 2023;46(10):2280–92.
11. Wang L, Zhu Q, Lu A, Liu X, Zhang L, Xu C, et al. Sodium butyrate suppresses angiotensin II-induced hypertension by Inhibition of renal (pro)renin receptor and intrarenal renin-angiotensin system. J Hypertens. 2017;35(9):1899–908.
12. Gotoh K, Shibata H. Association between the gut Microbiome and the renin-angiotensin-aldosterone system: a possible link via the activation of the immune system. Hypertens Res. 2023;46(10):2315–7.
13. Samochatova EV, Baidun LV, Rumiantsev AG, Korkina LG, Suslova TB. [Comparative study of the cytochemical, immunological and chemiluminescent indices of the blood and bone marrow cells in acute lympholeukemia]. Gematol Transfuziol. 1987;32(2):35–9.
14. Gomaa EZ. Human gut microbiota/microbiome in health and diseases: a review. Antonie Van Leeuwenhoek. 2020;113(12):2019–40.
15. Rashidah NH, Lim SM, Neoh CF, Majeed ABA, Tan MP, Khor HM, et al. Differential gut microbiota and intestinal permeability between frail and healthy older adults: A systematic review. Ageing Res Rev. 2022;82:101744.
16. Maslennikov R, Poluektova E, Zolnikova O, Sedova A, Kurbatova A, Shulpekova Y et al. Gut microbiota and bacterial translocation in the pathogenesis of liver fibrosis. Int J Mol Sci. 2023;24(22).
17. Komatsu S, Yokoyama Y, Nagino M. Gut microbiota and bacterial translocation in digestive surgery: the impact of probiotics. Langenbecks Arch Surg. 2017;402(3):401–16.
18. Tapper EB, Parikh ND. Diagnosis and management of cirrhosis and its complications: A review. JAMA. 2023;329(18):1589–602.
19. Wong CL, Holroyd-Leduc J, Thorpe KE, Straus SE. Does this patient have bacterial peritonitis or portal hypertension? How do I perform a paracentesis and analyze the results? JAMA. 2008;299(10):1166–78.
20. Biggins SW, Angeli P, Garcia-Tsao G, Gines P, Ling SC, Nadim MK, et al. Diagnosis, evaluation, and management of Ascites, spontaneous bacterial peritonitis and hepatorenal syndrome: 2021 practice guidance by the American association for the study of liver diseases. Hepatology. 2021;74(2):1014–48.
21. Yang Q, Bae G, Nadiradze G, Castagna A, Berezhnoy G, Zizmare L, et al. Acidic Ascites inhibits ovarian cancer cell proliferation and correlates with the metabolomic, lipidomic and inflammatory phenotype of human patients. J Transl Med. 2022;20(1):581.
22. Xuan Y, Wang H, Yung MM, Chen F, Chan WS, Chan YS, et al. SCD1/FADS2 fatty acid desaturases equipoise lipid metabolic activity and redox-driven ferroptosis in ascites-derived ovarian cancer cells. Theranostics. 2022;12(7):3534–52.
23. Sumner LW, Amberg A, Barrett D, Beale MH, Beger R, Daykin CA, et al. Proposed minimum reporting standards for chemical analysis chemical analysis working group (CAWG) metabolomics standards initiative (MSI). Metabolomics. 2007;3(3):211–21.
24. Wishart DS, Oler E, Peters H, Guo A, Girod S, Han S, et al. MiMeDB: the human microbial metabolome database. Nucleic Acids Res. 2023;51(D1):D611–20.
25. Parsons SL, Watson SA, Steele RJ. Malignant Ascites. Br J Surg. 1996;83(1):6–14.
26. Sangisetty SL, Miner TJ. Malignant ascites: A review of prognostic factors, pathophysiology and therapeutic measures. World J Gastrointest Surg. 2012;4(4):87–95.
27. Kipps E, Tan DS, Kaye SB. Meeting the challenge of Ascites in ovarian cancer: new avenues for therapy and research. Nat Rev Cancer. 2013;13(4):273–82.
28. Brown PD. Matrix metalloproteinase inhibitors: a novel class of anticancer agents. Adv Enzyme Regul. 1995;35:293–301.
29. Beattie GJ, Smyth JF. Phase I study of intraperitoneal metalloproteinase inhibitor BB94 in patients with malignant Ascites. Clin Cancer Res. 1998;4(8):1899–902.
30. Schwabe RF, Jobin C. The Microbiome and cancer. Nat Rev Cancer. 2013;13(11):800–12.
31. Grivennikov SI. Inflammation and colorectal cancer: colitis-associated neoplasia. Semin Immunopathol. 2013;35(2):229–44.
32. Zhao Y, Yu YB. Intestinal microbiota and chronic constipation. Springerplus. 2016;5(1):1130.
33. Schwabl P, Hambruch E, Seeland BA, Hayden H, Wagner M, Garnys L, et al. The FXR agonist PX20606 ameliorates portal hypertension by targeting vascular remodelling and sinusoidal dysfunction. J Hepatol. 2017;66(4):724–33.
34. Munoz L, Borrero MJ, Ubeda M, Conde E, Del Campo R, Rodriguez-Serrano M, et al. Intestinal immune dysregulation driven by dysbiosis promotes barrier disruption and bacterial translocation in rats with cirrhosis. Hepatology. 2019;70(3):925–38.
35. Lynch SV, Pedersen O. The human intestinal Microbiome in health and disease. N Engl J Med. 2016;375(24):2369–79.
36. Ahmed N, Stenvers KL. Getting to know ovarian cancer ascites: opportunities for targeted therapy-based translational research. Front Oncol. 2013;3:256.
37. Krugmann J, Schwarz CL, Melcher B, Sterlacci W, Ozalinskaite A, Lermann J, et al. Malignant Ascites occurs most often in patients with high-grade serous papillary ovarian cancer at initial diagnosis: a retrospective analysis of 191 women treated at Bayreuth hospital, 2006–2015. Arch Gynecol Obstet. 2019;299(2):515–23.
38. Mikula-Pietrasik J, Uruski P, Szubert S, Szpurek D, Sajdak S, Tykarski A, et al. Malignant Ascites determine the transmesothelial invasion of ovarian cancer cells. Int J Biochem Cell Biol. 2017;92:6–13.
39. Neurauter G, Schrocksnadel K, Scholl-Burgi S, Sperner-Unterweger B, Schubert C, Ledochowski M, et al. Chronic immune stimulation correlates with reduced phenylalanine turnover. Curr Drug Metab. 2008;9(7):622–7.
40. Dahiya R, Boyle B, Goldberg BC, Yoon WH, Konety B, Chen K, et al. Metastasis-associated alterations in phospholipids and fatty acids of human prostatic adenocarcinoma cell lines. Biochem Cell Biol. 1992;70(7):548–54.
41. Radin NS. Cancer progression in the kidney and prostate: vital roles of sphingolipids in chemotherapy. Urology. 2002;60(4):562–8.
42. Zheng K, Chen Z, Feng H, Chen Y, Zhang C, Yu J, et al. Sphingomyelin synthase 2 promotes an aggressive breast cancer phenotype by disrupting the homoeostasis of ceramide and sphingomyelin. Cell Death Dis. 2019;10(3):157.
43. Marchesini N, Osta W, Bielawski J, Luberto C, Obeid LM, Hannun YA. Role for mammalian neutral Sphingomyelinase 2 in confluence-induced growth arrest of MCF7 cells. J Biol Chem. 2004;279(24):25101–11.
44. Jing F, Jing C, Dai X, Zhou G, Di S, Bi X, et al. Sphingomyelin synthase 2 but not sphingomyelin synthase 1 is upregulated in ovarian cancer and involved in migration, growth and survival via different mechanisms. Am J Transl Res. 2021;13(5):4412–21.
45. Committee on the State of the Science in Ovarian Cancer Research; Board on Health Care Services; Institute of Medicine. National academies of sciences E, and medicine. Ovarian cancers: evolving paradigms in research and care. Washington (DC): National Academies Press (US); 2016.

46. Eriksen R, Perez IG, Posma JM, Haid M, Sharma S, Prehn C, et al. Dietary metabolite profiling brings new insight into the relationship between nutrition and metabolic risk: an IMI DIRECT study. EBioMedicine. 2020;58:102932.
47. Khanlarkhani N, Azizi E, Amidi F, Khodarahmian M, Salehi E, Pazhohan A, et al. Metabolic risk factors of ovarian cancer: a review. JBRA Assist Reprod. 2022;26(2):335–47.
48. Ford CE, Werner B, Hacker NF, Warton K. The untapped potential of Ascites in ovarian cancer research and treatment. Br J Cancer. 2020;123(1):9–16.
49. Rinninella E, Raoul P, Cintoni M, Franceschi F, Miggiano GAD, Gasbarrini A et al. What is the healthy gut microbiota composition?? A changing ecosystem across age, environment, diet, and diseases. Microorganisms. 2019;7(1).
50. Krautkramer KA, Fan J, Backhed F. Gut microbial metabolites as multi-kingdom intermediates. Nat Rev Microbiol. 2021;19(2):77–94.
51. O'Keefe SJ. Diet, microorganisms and their metabolites, and colon cancer. Nat Rev Gastroenterol Hepatol. 2016;13(12):691–706.
52. Dalal N, Jalandra R, Bayal N, Yadav AK, Harshulika, Sharma M, et al. Gut microbiota-derived metabolites in CRC progression and causation. J Cancer Res Clin Oncol. 2021;147(11):3141–55.
53. Banerjee S, Moore KN, Colombo N, Scambia G, Kim BG, Oaknin A, et al. Maintenance Olaparib for patients with newly diagnosed advanced ovarian cancer and a BRCA mutation (SOLO1/GOG 3004): 5-year follow-up of a randomised, double-blind, placebo-controlled, phase 3 trial. Lancet Oncol. 2021;22(12):1721–31.
54. Moore K, Colombo N, Scambia G, Kim BG, Oaknin A, Friedlander M, et al. Maintenance Olaparib in patients with newly diagnosed advanced ovarian Cancer. N Engl J Med. 2018;379(26):2495–505.
55. DiSilvestro P, Banerjee S, Colombo N, Scambia G, Kim BG, Oaknin A, et al. Overall survival with maintenance Olaparib at a 7-Year Follow-Up in patients with newly diagnosed advanced ovarian Cancer and a BRCA mutation: the SOLO1/GOG 3004 trial. J Clin Oncol. 2023;41(3):609–17.
56. Monk BJ, Parkinson C, Lim MC, O'Malley DM, Oaknin A, Wilson MK, et al. A randomized, phase III trial to evaluate Rucaparib monotherapy as maintenance treatment in patients with newly diagnosed ovarian Cancer (ATHENA-MONO/GOG-3020/ENGOT-ov45). J Clin Oncol. 2022;40(34):3952–64.
57. Lipson EJ, Sharfman WH, Drake CG, Wollner I, Taube JM, Anders RA, et al. Durable cancer regression off-treatment and effective reinduction therapy with an anti-PD-1 antibody. Clin Cancer Res. 2013;19(2):462–8.
58. Le DT, Uram JN, Wang H, Bartlett BR, Kemberling H, Eyring AD, et al. PD-1 Blockade in tumors with Mismatch-Repair deficiency. N Engl J Med. 2015;372(26):2509–20.
59. Overman MJ, McDermott R, Leach JL, Lonardi S, Lenz HJ, Morse MA, et al. Nivolumab in patients with metastatic DNA mismatch repair-deficient or microsatellite instability-high colorectal cancer (CheckMate 142): an open-label, multicentre, phase 2 study. Lancet Oncol. 2017;18(9):1182–91.
60. Overman MJ, Lonardi S, Wong KYM, Lenz HJ, Gelsomino F, Aglietta M, et al. Durable clinical benefit with nivolumab plus ipilimumab in DNA mismatch Repair-Deficient/Microsatellite Instability-High metastatic colorectal Cancer. J Clin Oncol. 2018;36(8):773–9.
61. Bang YJ, Van Cutsem E, Feyereislova A, Chung HC, Shen L, Sawaki A, et al. Trastuzumab in combination with chemotherapy versus chemotherapy alone for treatment of HER2-positive advanced gastric or gastro-oesophageal junction cancer (ToGA): a phase 3, open-label, randomised controlled trial. Lancet. 2010;376(9742):687–97.
62. Janjigian YY, Maron SB, Chatila WK, Millang B, Chavan SS, Alterman C, et al. First-line pembrolizumab and trastuzumab in HER2-positive oesophageal, gastric, or gastro-oesophageal junction cancer: an open-label, single-arm, phase 2 trial. Lancet Oncol. 2020;21(6):821–31.
63. Janjigian YY, Kawazoe A, Yanez P, Li N, Lonardi S, Kolesnik O, et al. The KEYNOTE-811 trial of dual PD-1 and HER2 Blockade in HER2-positive gastric cancer. Nature. 2021;600(7890):727–30.
64. Takahari D, Shoji H, Minashi K, Hara H, Chin K, Ooki A, et al. A phase Ib study of nivolumab plus trastuzumab with S-1/capecitabine plus oxaliplatin for HER2-positive advanced gastric cancer (Ni-HIGH study): safety evaluation. J Clin Oncol. 2020;38(15suppl):4525.
65. Garon EB, Rizvi NA, Hui R, Leighl N, Balmanoukian AS, Eder JP, et al. Pembrolizumab for the treatment of non-small-cell lung cancer. N Engl J Med. 2015;372(21):2018–28.
66. Ott PA, Bang YJ, Piha-Paul SA, Razak ARA, Bennouna J, Soria JC, et al. T-Cell-Inflamed Gene-Expression profile, programmed death ligand 1 expression, and tumor mutational burden predict efficacy in patients treated with pembrolizumab across 20 cancers: KEYNOTE-028. J Clin Oncol. 2019;37(4):318–27.
67. Villadolid J, Amin A. Immune checkpoint inhibitors in clinical practice: update on management of immune-related toxicities. Transl Lung Cancer Res. 2015;4(5):560–75.
68. Belum VR, Benhuri B, Postow MA, Hellmann MD, Lesokhin AM, Segal NH, et al. Characterisation and management of dermatologic adverse events to agents targeting the PD-1 receptor. Eur J Cancer. 2016;60:12–25.
69. Trinidad C, Nelson KC, Glitza Oliva IC, Torres-Cabala CA, Nagarajan P, Tetzlaff MT, et al. Dermatologic toxicity from immune checkpoint Blockade therapy with an interstitial granulomatous pattern. J Cutan Pathol. 2018;45(7):504–7.
70. Weber JS, Dummer R, de Pril V, Lebbe C, Hodi FS, Investigators MDX. Patterns of onset and resolution of immune-related adverse events of special interest with Ipilimumab: detailed safety analysis from a phase 3 trial in patients with advanced melanoma. Cancer. 2013;119(9):1675–82.
71. Dougan M. Checkpoint Blockade toxicity and immune homeostasis in the Gastrointestinal tract. Front Immunol. 2017;8:1547.
72. Abu-Sbeih H, Ali FS, Luo W, Qiao W, Raju GS, Wang Y. Importance of endoscopic and histological evaluation in the management of immune checkpoint inhibitor-induced colitis. J Immunother Cancer. 2018;6(1):95.
73. Zeissig S, Petersen BS, Tomczak M, Melum E, Huc-Claustre E, Dougan SK, et al. Early-onset Crohn's disease and autoimmunity associated with a variant in CTLA-4. Gut. 2015;64(12):1889–97.
74. Hammers HJ, Plimack ER, Infante JR, Rini BI, McDermott DF, Lewis LD, et al. Safety and efficacy of nivolumab in combination with ipilimumab in metastatic renal cell carcinoma: the checkmate 016 study. J Clin Oncol. 2017;35(34):3851–8.
75. Morad G, Helmink BA, Sharma P, Wargo JA. Hallmarks of response, resistance, and toxicity to immune checkpoint Blockade. Cell. 2021;184(21):5309–37.
76. Bodor JN, Boumber Y, Borghaei H. Biomarkers for immune checkpoint Inhibition in non-small cell lung cancer (NSCLC). Cancer. 2020;126(2):260–70.
77. Liu D, Schilling B, Liu D, Sucker A, Livingstone E, Jerby-Arnon L, et al. Integrative molecular and clinical modeling of clinical outcomes to PD1 Blockade in patients with metastatic melanoma. Nat Med. 2019;25(12):1916–27.
78. Routy B, Le Chatelier E, Derosa L, Duong CPM, Alou MT, Daillere R, et al. Gut Microbiome influences efficacy of PD-1-based immunotherapy against epithelial tumors. Science. 2018;359(6371):91–7.
79. Davar D, Dzutsev AK, McCulloch JA, Rodrigues RR, Chauvin JM, Morrison RM, et al. Fecal microbiota transplant overcomes resistance to anti-PD-1 therapy in melanoma patients. Science. 2021;371(6529):595–602.
80. Blake SJ, James J, Ryan FJ, Caparros-Martin J, Eden GL, Tee YC, et al. The immunotoxicity, but not anti-tumor efficacy, of anti-CD40 and anti-CD137 immunotherapies is dependent on the gut microbiota. Cell Rep Med. 2021;2(12):100464.
81. Marzio L, Neri M, Di Giammarco AM, Cuccurullo F, Lanfranchi GA. Dopamine-induced migrating myoelectrical complex-like activity in human duodenum. Dig Dis Sci. 1986;31(4):349–54.
82. Marzio L, Neri M, Pieramico O, Delle Donne M, Peeters TL, Cuccurullo F. Dopamine interrupts Gastrointestinal fed motility pattern in humans. Effect on motilin and somatostatin blood levels. Dig Dis Sci. 1990;35(3):327–32.
83. Singh B, Mal G, Marotta F. Designer probiotics: paving the way to living therapeutics. Trends Biotechnol. 2017;35(8):679–82.
84. Knuplez E, Marsche G. An updated review of Pro- and Anti-Inflammatory properties of plasma lysophosphatidylcholines in the vascular system. Int J Mol Sci. 2020;21(12).
85. Nie J, Zhang L, Zhao G, Du X. Quercetin reduces atherosclerotic lesions by altering the gut microbiota and reducing atherogenic lipid metabolites. J Appl Microbiol. 2019;127(6):1824–34.
86. Sasidharan Pillai S, Gagnon CA, Foster C, Ashraf AP. Exploring the gut microbiota: key insights into its role in obesity, metabolic syndrome, and type 2 diabetes. J Clin Endocrinol Metab. 2024;109(11):2709–19.
87. Heaver SL, Le HH, Tang P, Basle A, Mirretta Barone C, Vu DL, et al. Characterization of inositol lipid metabolism in gut-associated Bacteroidetes. Nat Microbiol. 2022;7(7):986–1000.
88. Parada Venegas D, De la Fuente MK, Landskron G, Gonzalez MJ, Quera R, Dijkstra G, et al. Short chain fatty acids (SCFAs)-Mediated gut epithelial and immune regulation and its relevance for inflammatory bowel diseases. Front Immunol. 2019;10:277.
89. Naudin S, Sampson JN, Moore SC, Albanes D, Freedman ND, Weinstein SJ, et al. Lipidomics and pancreatic cancer risk in two prospective studies. Eur J Epidemiol. 2023;38(7):783–93.
90. Hannun YA, Obeid LM. Principles of bioactive lipid signalling: lessons from sphingolipids. Nat Rev Mol Cell Biol. 2008;9(2):139–50.

91. Hannun YA, Bell RM. Lysosphingolipids inhibit protein kinase C: implications for the sphingolipidoses. Science. 1987;235(4789):670–4.
92. Dressler KA, Mathias S, Kolesnick RN. Tumor necrosis factor-alpha activates the sphingomyelin signal transduction pathway in a cell-free system. Science. 1992;255(5052):1715–8.
93. Ala M. Tryptophan metabolites modulate inflammatory bowel disease and colorectal cancer by affecting immune system. Int Rev Immunol. 2022;41(3):326–45.
94. Oellgaard J, Winther SA, Hansen TS, Rossing P, von Scholten BJ. Trimethylamine N-oxide (TMAO) as a new potential therapeutic target for insulin resistance and Cancer. Curr Pharm Des. 2017;23(25):3699–712.
95. Liu CT, Raghu R, Lin SH, Wang SY, Kuo CH, Tseng YJ, et al. Metabolomics of ginger essential oil against alcoholic fatty liver in mice. J Agric Food Chem. 2013;61(46):11231–40.
96. Clendening JW, Pandyra A, Boutros PC, El Ghamrasni S, Khosravi F, Trentin GA, et al. Dysregulation of the mevalonate pathway promotes transformation. Proc Natl Acad Sci U S A. 2010;107(34):15051–6.
97. Huang B, Song BL, Xu C. Cholesterol metabolism in cancer: mechanisms and therapeutic opportunities. Nat Metab. 2020;2(2):132–41.
98. Dai X, Zhu BT. Suppression of T-cell response and prolongation of allograft survival in a rat model by Tryptophan catabolites. Eur J Pharmacol. 2009;606(1–3):225–32.
99. Lee K, Kwak JH, Pyo S. Inhibition of LPS-induced inflammatory mediators by 3-hydroxyanthranilic acid in macrophages through suppression of PI3K/NF-kappaB signaling pathways. Food Funct. 2016;7(7):3073–82.
100. Fiore A, Murray PJ. Tryptophan and Indole metabolism in immune regulation. Curr Opin Immunol. 2021;70:7–14.
101. Yang J, Liu L, Li M, Huang X, Yang H, Li K. Naringenin inhibits pro–inflammatory cytokine production in macrophages through inducing MT1G to suppress the activation of NF–kappaB. Mol Immunol. 2021;137:155–62.
102. Rehman MU, Rahman Mir MU, Farooq A, Rashid SM, Ahmad B, Bilal Ahmad S, et al. Naringenin (4,5,7-trihydroxyflavanone) suppresses the development of precancerous lesions via controlling hyperproliferation and inflammation in the colon of Wistar rats. Environ Toxicol. 2018;33(4):422–35.
103. Cai J, Wen H, Zhou H, Zhang D, Lan D, Liu S, et al. Naringenin: A Flavanone with anti-inflammatory and anti-infective properties. Biomed Pharmacother. 2023;164:114990.
104. Jin L, Zeng W, Zhang F, Zhang C, Liang W. Naringenin ameliorates acute inflammation by regulating intracellular cytokine degradation. J Immunol. 2017;199(10):3466–77.
105. Abotaleb M, Samuel SM, Varghese E, Varghese S, Kubatka P, Liskova A et al. Flavonoids in Cancer and apoptosis. Cancers (Basel). 2018;11(1).
106. Yahfoufi N, Alsadi N, Jambi M, Matar C. The Immunomodulatory and Anti-Inflammatory role of polyphenols. Nutrients. 2018;10(11).
107. Lane D, Matte I, Garde-Granger P, Bessette P, Piche A. Ascites IL-10 promotes ovarian Cancer cell migration. Cancer Microenviron. 2018;11(2–3):115–24.
108. Ito T, Hanafusa N, Iwase S, Noiri E, Nangaku M, Nakagawa K, et al. Ascitic IL-10 concentration predicts prognosis of patients undergoing Cell-Free and concentrated Ascites reinfusion therapy. Ther Apher Dial. 2020;24(1):90–5.
109. Tao Y, Zhang Q, Huang W, Zhu H, Zhang D, Luo W. The peritoneal leptin, MCP-1 and TNF-alpha in the pathogenesis of endometriosis-associated infertility. Am J Reprod Immunol. 2011;65(4):403–6.
110. Ulukus M, Ulukus EC, Tavmergen Goker EN, Tavmergen E, Zheng W, Arici A. Expression of interleukin-8 and monocyte chemotactic protein 1 in women with endometriosis. Fertil Steril. 2009;91(3):687–93.
111. Kharfi A, Akoum A. Correlation between decreased type-II interleukin-1 receptor and increased monocyte chemotactic protein-1 expression in the endometrium of women with endometriosis. Am J Reprod Immunol. 2001;45(4):193–9.

Publisher's note

Springer Nature remains neutral with regard to jurisdictional claims in published maps and institutional affiliations.